## Basic idea about nanomaterials

MSc -Semester IV

(Course -CHE-CC-428)

### Dr. Pushpal Ghosh

**Assistant Professor** 

(Alexander von Humboldt Fellow)

School of Chemical Science and Technology,
Department of Chemistry
Dr. Harisingh Gour Vishwavidyalaya
(A Central University)
Sagar-470003, Madhya Pradesh

### 1.1 Origin of nanomaterials

In recent times, engineering the structure and properties of nano-sized materials for numerous applications is getting tremendous attention (**Figure 1**).

The term 'nano' has been derived from the Greek words 'Nanos' meaning dwarf or small size. Nano means 10<sup>-9</sup> where 1 nanometer is equivalent to one thousandth of a micrometer or one millionth of a millimeter or one billionth of a meter. On reducing the size of particle from bulk to nano, physical and chemical properties (i.e. electronic, magnetic, catalytic, melting and optical etc.) are drastically modified compared to their bulk counterpart. 1-9 Size of nanoparticles is intermediate between small molecule of nanomaterials in different fields. and bulk metal.<sup>2,7</sup>

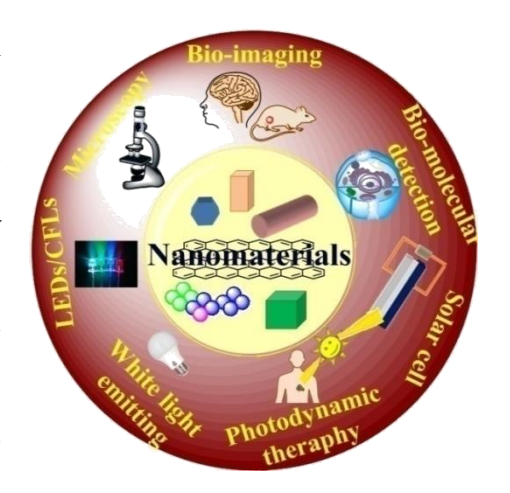


Figure 1. Schematic representation

Thus, the resulting properties are neither shown by its molecular compounds nor by the respective bulk. A famous quote stated long ago by Wolfgang Pauli, which says: 10

### "God made the bulk, the surface was invented by the Devil".

All the properties (including physical and chemical properties) generated due to miniaturization are becoming the surface-dependent property. 11,12 It is related to the number of atoms exposed to the surrounding of bulk and of the nanoscale-size particles. On reducing the size of materials from bulk to the nano-size regime, number of atoms in contact of external environment also increases as compared to the bulk. 11 As a resulting, physical and chemical properties of nano-sized particles are dramatically modified compared to their bulk analogoue.8,11,12

Exploration of different properties due to nanoscale miniaturization is started in 19th century, when size dependent phenomenon was first time noticed by Michael Faraday in 1858. 13-14 He found that on reducing the size of gold sol to nanoscale regime, the electronic and optical properties were completely different compared to the bulk gold metal. However, size dependent physical properties of gold sol at that time were not illustrated. 13-15

There are several examples from which effect of size on the bulk properties can be seen. For instances, gold is yellowish, lustrous and inert element in the bulk and is highly used for making the jewelries. However, at nanoscale regime its color is turned to red, becoming highly reactive and efficient catalyst for catalyzing many chemical reactions. 15-16 Similarly,

Pt and Pd are non-magnetic materials in the bulk but exhibit considerable magnetic properties in few atoms cluster owing to the presence of large number of unpaired electrons on the entire particle surface. <sup>17-19</sup> Similarly, silver particles of nanoscale regime have widespread applications and it is not only utilized for catalyzing the numerous reactions but also shows luminescence property. <sup>20</sup> In 20<sup>th</sup> century, Richard Adolf Zsigmondy noticed optical behavior of numerous colloidal suspension and light scattering process by the tiniest noble metal particles using the optical microscope and dark field illumination which was termed as ultramicroscope. <sup>21</sup> Improvement of electron microscopic techniques with time also enhanced the understanding about nanoscale phenomenon. Miniaturizations of material and electronic devices using nanotechnology and nanoscience open the new door for mankind for efficiently

Feynman proposed inspiring ideas to all scientific community in his lecture entitled as "There is a plenty of room at the bottom".<sup>22</sup> He illustrated that there would be a new world at the nanoscale size where the behavior of particles would be completely different compared to their bulk and their constituent (atom). Later, Norio Taniguchi of the Tokyo Science University defined the term nanotechnology.<sup>23</sup> In1980s, Brus and Ekimov illustrated the relation between size of nanocrystallite and their optical properties.<sup>2,24</sup> In 1982, Henglein and Gratzel, used the CdS as catalyst and photosensitizers.<sup>25-26</sup> The major breakthrough

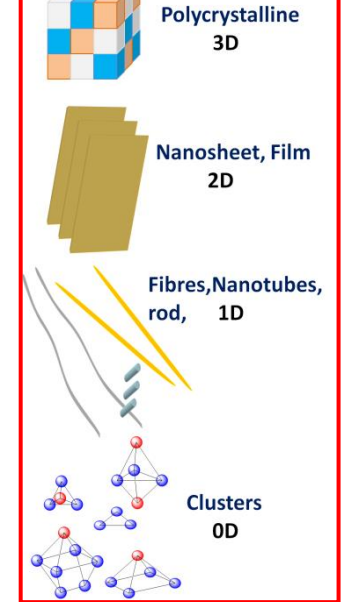


Figure 2: Size of structural elements of nanocrystalline materials.

in the field of nanotechnology taken place in 1985 when Curl, Kroto, and Smalley discovered other allotropes of carbon which is famously called fullerenes.<sup>27</sup> Few years later, in 1991, Sumio

Ijima discovered multiwall carbon nanotubes (MWNT) and then in 1993 single wall carbon nanotubes (SWNT) was synthesized by Donald Bethune *et al.*<sup>28-29</sup> This was actually the cylindrical form of single layer graphene and these have high electrical and mechanical strength. In 95<sup>th</sup> Indian Science Congress, Nobel laureate Robert Curl Jr. mentioned that nanotechnology was extensively used by Indian craftsmen and artisans about 2000 years ago when they have painted the walls of the monolithic caves of Ajanta and Ellora. On other hand, another boost in the field of nanoscience was the discovery of graphene in 2004 by K.S. Novoselov and A.K. Geim of University of Manchester, which is a single atom thick, two dimensional (2D) material.<sup>30</sup> It was prepared by very simple micromechanical cleavage

of graphite using the scotch tape. Now this 2D material has significantly impacted on the nanoscience and nanotechnology.

On the basis of morphology and physical properties, nanomaterials can be further classified into different categories. For instances, it may be 0D, 1D, 2D and 3D on the basis of dimension which can be controlled during the growth of nanoparticles (**Figure 2**).<sup>4,31-32</sup> All the dimensions which are restricted in nanoscale regime (≤10 nm) is called 0D like quantum dots. In 1D nanomaterial, one of the dimensions is not included in nanoscale such as nanofibres, nanotubes and rods. <sup>4,31-32</sup> These fibres, rod and tubes have length from 100 nm to few microns. In 2D nanomaterials, their two of the dimensions are not confined to the nanoscale. These nanomaterials contains film or sheet like structure which have nanometer thickness for examples graphene, film coated on the substrates etc. However the three dimensional nanostructures are composed of nanosize grains which form owing to the agglomeration of nanoparticles and often observed in nanopowders etc.<sup>4,31-32</sup>

### 1.2 Evolution of luminescence phenomenon

Nanomaterials have various physical and chemical properties and amongst them luminescence property is one of the most fascinating property. Luminescence is emission of light by substance.<sup>33</sup> Sometime, it is also called cold body radiation emission.<sup>34</sup> This process is attributed to chemical reaction, electrical energy, motion of sub-atomic particles and mechanical strain on the materials.<sup>34</sup> There are different types of luminescence process on the basis of physical and chemical processes such as chemiluminescence, thermoluminescence, photoluminescence, mechanoluminescence and so on.<sup>34-35</sup>

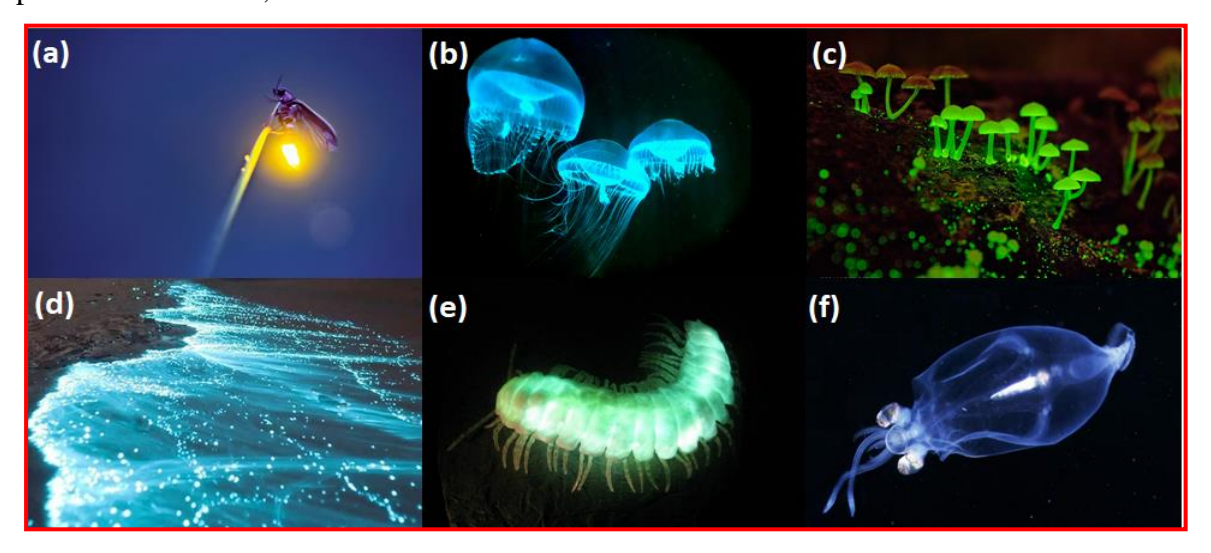


**Figure 3:** Bioluminescence images of a) firefly, b) jelly fish, c) fungi, d) zooplanktons and phytoplanktons e) insects and f) squid.<sup>41-46</sup>

In our nature, there are lots of examples where one can see this process with naked eyes. The most common example of luminescence is firefly which seems to be glow in the night. <sup>36-38</sup> Besides, marine animals such as jelly fishes, sea urchin, sea anemones, fungi, zooplanktons and phytoplanktons also show the luminescence process (**Figure 3**). <sup>39-40</sup> This is also known as bioluminescence; which actually comes under the chemiluminescence process, since, these luminescence processes occur due to the chemical reaction. For example in case of firefly, during the chemical reaction, luciferin (L) molecules get oxidized in the presence of oxygen molecules, Mg<sup>2+</sup> and Luciferase enzyme by expensing of adenosine triphosphate (ATP), and then converted to Oxy-luciferin which shows luminescence (as shown in **figure 4**). <sup>36-37</sup>

Figure 4: Oxidation of luciferin molecule to luminescent oxy-luciferin molecule.

Different organisms have different types of luciferin molecules and it varies from species to species.<sup>36-39</sup> However, the origin of luminescence in materials especially nanoscale particles is completely different than that of bioluminescence.

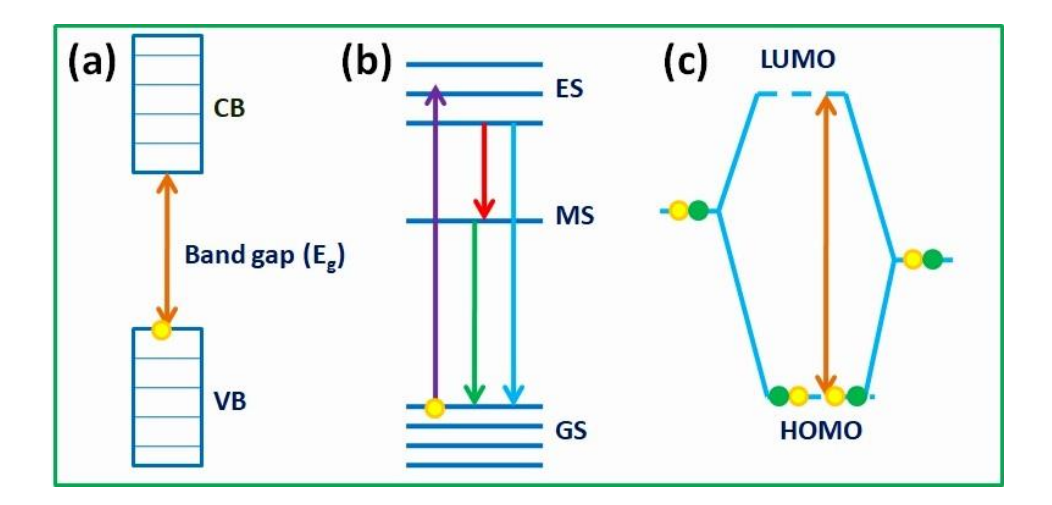


**Figure 5:** Electronic transition in different nanomaterials a) semiconductor b) rare-earth doped and c) organic based.

Usually, three classes of luminescent materials have been explored so far, for instances semiconducting, rare-earth ion doped (RE) and organic based luminescent nanomaterials. In these materials luminescence process is fundamentally occurred due to electronic transition taken place from valance band (VB) to conduction band (CB), in different metastable states (MS) situated between the ground state (GS) and excited state (ES) and from highest occupied molecular orbitals (HOMO) to lowest unoccupied molecular orbitals (LUMO) in conjugated system of semiconducting, rare-earth doped nanomaterials and organic based luminescent materials respectively (**Figure 5**). <sup>1-3,11,13</sup> Several factors that govern the luminescence property of nanomaterials will be discussed in later sections.

### 1.2.1 Rare-Earth ion (RE<sup>3+</sup>) Doped Luminescent Nanomaterials

In periodic table, there are seventeen elements such as scandium, yttrium, lanthanum and fourteen elements of lanthanide series i.e. from cerium to lutetium are known as rare-earth elements due to their less abundance in earth. These are commonly occurred in III (+3) oxidation state which can be generally represented as  $RE^{3+}$  and their electronic configuration can be expressed as  $[Xe] 4f^n$ .

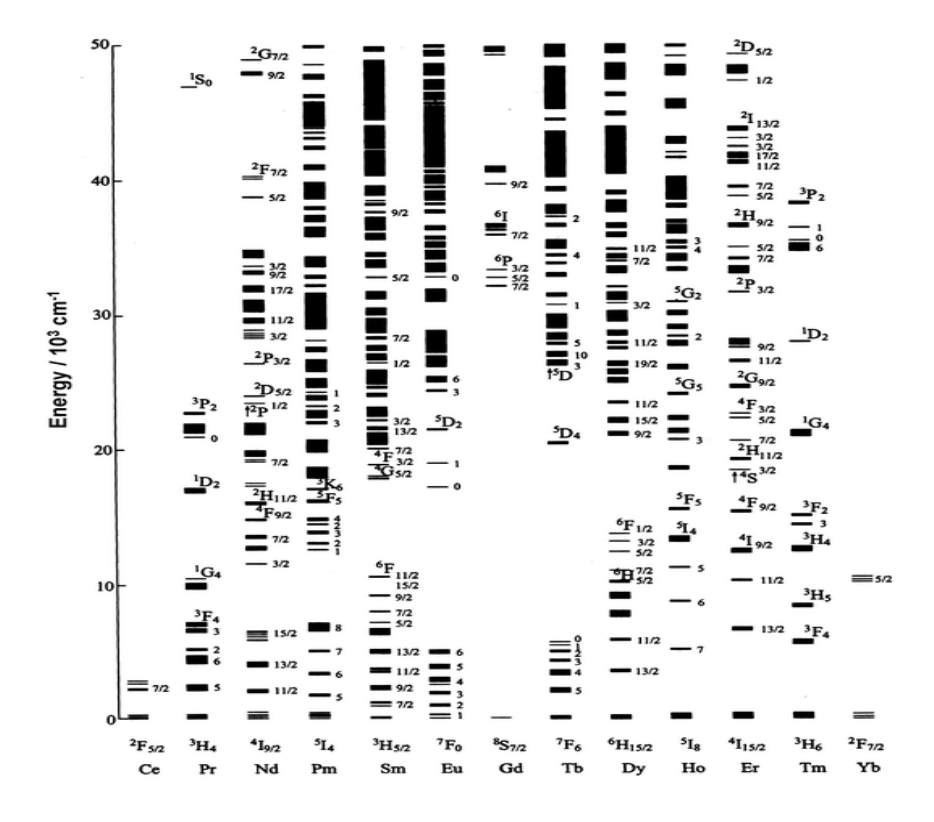
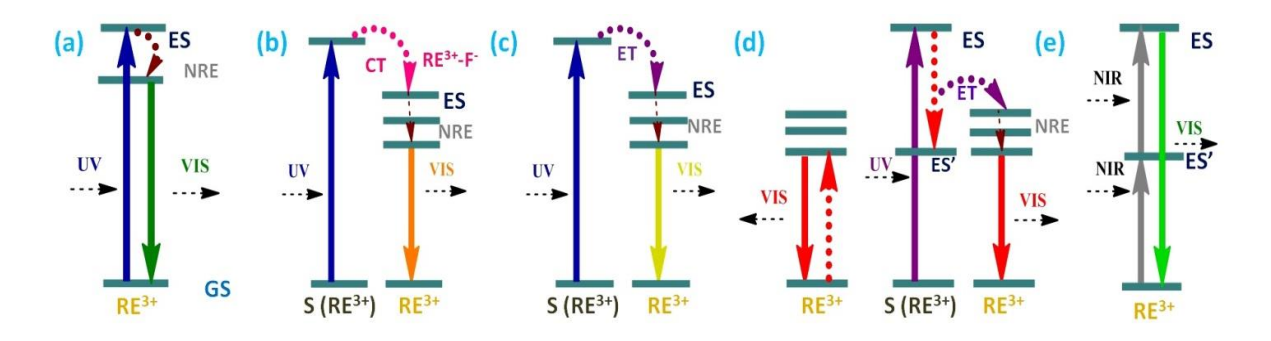


Figure 6: Energy levels of rare-earth ions (RE<sup>3+</sup>). 48,49

Origin of luminescence centre in RE<sup>3+</sup> is due to spin orbit coupling (2J+1) degenerate J-levels splitting, leading to generation of rich quantities of high electronic energy levels (excited state) (**Figure 6**). However, extent of splitting is less than d-orbital splitting of transition metals.  $^{47-50}$  Number of allowed electronic energy levels can be calculated using the equation 14!/(14-n)!n!, where n is the number of electrons in the 4f-orbitals of RE<sup>3+</sup> ions.  $^{47-50}$  These intraconfigurational f-f electronic transitions are parity forbidden and well shielded by high energy filled  $5s^25p^6$  orbitals. As a result, there is no effect of external ligand field strength on the f-f electronic transitions.  $^{47-50}$  Thus, their excitation and emission position is definite and it is not influenced by quantum confinement effect, unlike semiconductors in which luminescence process is dependent on size dependent band gap.  $^{51-53}$  On the other hand, in organic based luminescent nanomaterials, it is a function of HOMO-LUMO conjugation length.  $^{49-50}$  Amongst RE elements, La<sup>3+</sup> and Lu<sup>3+</sup> do not show any luminescence which is attributed to either empty or completely filled 4f-orbitals.  $^{48}$ 



**Figure 7.** Schematic representation of different types of photo-physical dynamics of RE doped nanoparticles: a) simple direct excitation, b) charge transfer, c) energy transfer, d) quantum cutting downconversion, e) excited state upconversion (ESU).<sup>47-48</sup>

Owing to doping of single or combination of RE ion/s, numerous luminescent centers are generated. As a result, several types of photodynamic process are taken place (**Figure 7**). For instances, singly doped rare-earth ion shows simple f-f electronic transition in which electron is directly excited from ground state to excited state. By non-radiative emission, it comes to lower level of excited state and then via radiative emission it relaxes to ground state. A7-50 In addition of f-f transition, RE ions also show two other types of electronic transitions like f-f-f and charge transfer. f-f-f electronic transition is spin allowed and its emission intensity is very much susceptible to the external environment. While, charge-transfer transition such as ligand to metal charge transfer (LMCT) is obtained at higher energy (typically f-f-f electronic transition may except Eu<sup>3+</sup>, Yb<sup>3+</sup> and sometime Sm<sup>3+</sup> and Tm<sup>3+</sup>) compared to f-f-f-electronic transition

process. Thus, direct excitation is forbidden, and although being low absorption coefficient, less energy is required for exciting the RE ions than excitation via charge transfer process. In this way, luminescent feature of RE ions is notably dependent on excitation process. To overcome this problem, sensitizers (Ce<sup>3+</sup> and Yb<sup>3+</sup>) are used which have high absorption cross-section. Generally, sensitizers absorb the energy from the source and transfer it to the activator which finally emits the absorbed energy in terms of radiative emission. Other photodynamic processes such as energy transfer, quantum cutting down conversion and upconversion are also found. These processes take place due to judicious doping of combination of RE ions like in energy transfer process, for example one in which Ce<sup>3+</sup> and Tb<sup>3+</sup> ions are doped together.

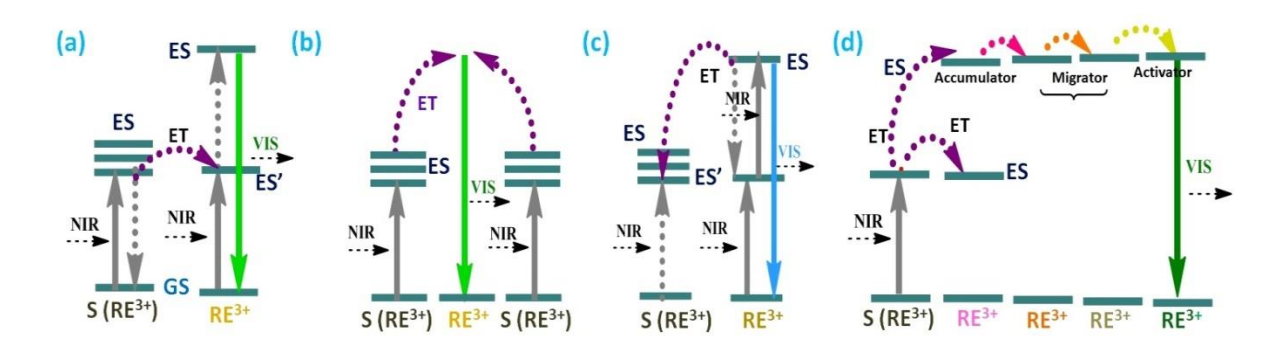


**Figure 8.** Different types of upconversion processes: a) energy transfer upconversion (ETU), b) co-operative energy transfer upconversion (CEU), c) photon avalanche upconversion (PAU) and d) energy migration mediated upconversion (EMU). 47-48

The emission spectrum of  $Ce^{3+}$  is nicely overlapped with the absorption spectrum of  $Tb^{3+}$ .<sup>48</sup>, <sup>54</sup> Singly doped  $Ce^{3+}$  ions doped nanophosphors emit violet color. However, in  $Ce^{3+}$  and  $Tb^{3+}$  ions doped host matrix, on exciting the  $Ce^{3+}$  ions, energy transfer is occurred form  $Ce^{3+}$  ions to  $Tb^{3+}$  ions. Despite of violet color, now emission is occurred in green region of light which is emitted by  $Tb^{3+}$  ions. The extent of energy transfer can be determined using  $\eta_{et} = (1-I_d/I_{do})x100$ ; where  $\eta_{et}$  is energy transfer efficiency (%),  $I_{do}$  and  $I_d$  is the luminescence emission intensity by donor in the absence and presence of acceptor.<sup>54</sup> In this process,  $Ce^{3+}$  ions acts as energy donor and  $Tb^{3+}$  acts as energy acceptor.<sup>54</sup> On the other hand, in downconversion process, high energy single photon is converted approximately to two low energy photons; for example  $Eu^{3+}$  ions doped with  $GdF_3$  and  $NaGdF_4$ .<sup>57-60</sup> Conversely, upconversion process which was independently illustrated by Auzel as well as Ovsyankin and Feofilov, in which low energy excitation photon is converted into high energy singly emitted photon.<sup>47-48,51,61</sup> This is attributed to presence of at least two real metastable states in between

the ground and excited states. Upconversion process can be further divided into five categories (Figure 7e and 8): (a) excited state absorption (ESA), (b) energy transfer upconversion (ETU), (c) co-operative energy transfer upconversion (CET), (d) mediated photon-avalanche effect (PA) and (e) energy migration upconversion (EMU). 48,62 In UC photodynamic processes, Yb<sup>3+</sup> ions are commonly employed as sensitizer (S), however, Er <sup>3+</sup>, Ho<sup>3+</sup> and Tm<sup>3+</sup> ions are doped as activators. Interestingly, Gd<sup>3+</sup> ion is also incorporated along with Yb3+, Tm3+ and other RE3+ ions (RE3+~ Eu3+ and Tb3+) in EMU process which was discovered by Wang et al.<sup>62</sup> In EMU process, on the basis of their response toward irradiated energy, dopant ions can be further classified as sensitizer (absorbing the energy, Yb3+), accumulator (storing the energy, Tm<sup>3+</sup>), migrator (transferring the energy, Gd<sup>3+</sup>) and activator (emitting the absorbed energy, Eu<sup>3+</sup>/Tb<sup>3+</sup>). 48,62

However, these photodynamic processes of RE ions are extensively dependent on the several factors including judicious selection of host materials, tuning the crystal phase, shape, coreshell and lattice strain (Figure 9) etc. 48,63-64 Earlier, luminescent properties of RE ions are

studied by forming the inorganic-organic metal complexes.<sup>50</sup> However, due to their less chemical and physical stability, applications of these materials was limited.<sup>50</sup> Thereafter, RE ions were used to dope in inorganic host matrixes. 49-50 Generally, it is noticed that host matrix plays a crucial role in tuning the luminescence intensity of RE ions doped nanomaterial.<sup>48</sup> Unlike semiconductors based photoluminescence, position of emission centre in rare-earth based nanomaterials is fixed. It means emission position is not changed with varying the host matrix. On the other hand, only intensity of doped nanoparticles.

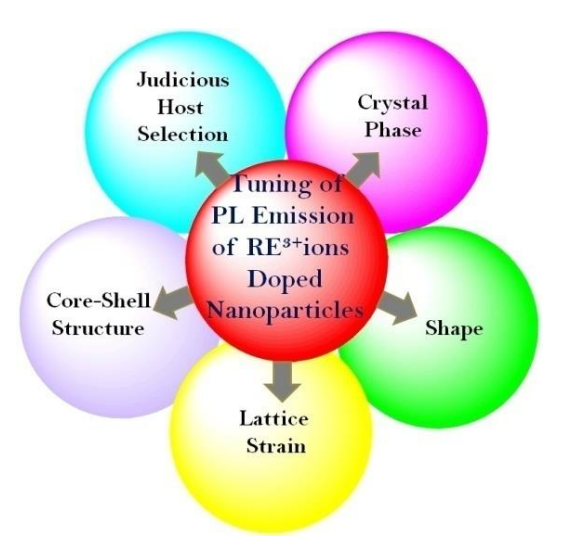


Figure 9. Schematic representation of factors influencing photoluminescence dynamics of RE

emission spectrum or sometimes the ratio between the different peaks in a spectrum is increased or decreased. So judicious selection of host matrix is very important for doping of RE ions. 47-48 To date, there are several inorganic host matrixes which have been explored for doping of RE ions for instances oxides, phosphates, alkali and alkaline-earth metal based binary and ternary fluorides, vanadate and sulphides etc. 47-48 Amongst those, recently fluoride based host matrixes are substantially used for doping of different RE ions due to large band

gap, high refractive index, less phonon energy and most importantly high chemical and thermal stability. In addition, crystal phase of host matrix is also playing the pivotal role in augmenting the luminescence property of the host materials. A7-48 Several physical and chemical factors have been noticed for tuning the crystal phase of host materials such as temperature, size of RE<sup>3+</sup> ions, ratio of precursors and synthesis methods, dopant ion concentration, solvent composition during synthesis and most importantly chelating, capping and templating agents, only a few to name. A7-48 For examples, selective phase transition from cubic ( $\alpha$ ) to thermodynamically more stable hexagonal ( $\beta$ ) NaYF<sub>4</sub> nanocrystals was observed by Shan *et al.* A9 Phase transition was accompanied due to change in the composition of the solvent. On the other hand, Ghosh et al. elucidated that quantum efficiency (67%) of hexagonal ( $\beta$ ) Na (Y<sub>1.5</sub>Na<sub>0.5</sub>)F<sub>6</sub> was obtained higher than that of cubic NaYF<sub>4</sub> (15%) on direct excitation of the sample ( $\lambda_{ex}$ =394 nm). Shung *et al.* observed that luminescence intensity of orthorhombic EuF<sub>3</sub> was very weaker compared to the hexagonal EuF<sub>3</sub> nanocrystals.

On reducing the size of particles to nanoscale size, specific surface area increases and number of atoms on the surface increases compared to the bulk leading to co-ordination number of atoms is perturbed and unsatisfied bonds or dangling bond are more up on the surface. 47-48 These dangling bonds reduce the luminescence emission intensity. 47-48,67 For prevailing over this issue, core-shell structure was introduced, which enhances the luminescence intensity by reducing the dangling bonds and increasing the surface quencher distances from the emission centre. 68 Minimum lattice mismatch is the prerequisite for making the efficient core-shell structure leading to get the significantly enhanced luminescence. 48 For instances, Yi *et al.* observed that UC luminescence intensity of NaYF4 coated NaYF4:Yb, Er and NaYF4:Yb, Tm nanocrystals was increased ~7 and ~29 times respectively compared to their uncoated analogue. This enhancement in emission intensity is due to reduction of surface defects resulting of core-shell formation. 69

Morphology of nanoparticles has also very significant impact on the luminescence property of RE doped nanoparticles, especially shape, aspect ratio and size of nanoparticles. <sup>47-48</sup> Generally it is noticed that as the size of nanoparticles is reduced to certain range, surface defects increases leading to quenching of luminescence intensity. <sup>70</sup> For illustrating the effect of morphology of nanoparticles on the luminescence intensity, Mai *et al.* synthesized the various nanoparticles of NaEuF<sub>4</sub> having different morphologies such as nanorods, nanospheres and nanopolyhedra, and then comparative study of emission spectra was done on the basis of their different morphologies. <sup>71</sup> Europium is often used as spectroscopic probe, so

any change in its electronic environment leads to changes observed in its emission spectrum.<sup>71</sup> Shape and morphology dependent tuning of luminescence intensity of EuF<sub>3</sub> nanocrystal was also studied by Wang *et al.*<sup>72</sup> Xu and co-worker also depicted the effect of size and shape of microcrystals of LuF<sub>3</sub>:Yb<sup>3+</sup>/Er<sup>3+</sup> and LuF<sub>3</sub>:Yb<sup>3+</sup>/Ho<sup>3+</sup> which emitted in yellowish-green. It was found that their nanoparticles initially agglomerated to form shuttle-like and litchi-like microcrystal and subsequently surface defect was also reduced leading to the augmentation of luminescence intensity in the yellowish-green region.<sup>73</sup>

Another important factor i.e. lattice strain which is also contributing significant role in tuning the emission intensity of  $RE^{3+}$  ion(s) doped host matrix, and can be calculated using the Williamson–Hall equation:  $^{48,54,74-76}$ 

$$\frac{\beta \cos \theta}{\lambda} = \frac{1}{D} + \eta \frac{\sin \theta}{\lambda} \tag{1}$$

On plotting the graph between  $\beta\cos\theta/\lambda$  vs  $\sin\theta/\lambda$ , slope of the graph shows the lattice strain ( $\eta$ ) and crystallite size (D) can be determined from the intercept. Positive and negative magnitude of slope indicates the tensile and compressive strain of the lattice strain respectively. Tensile strain is defined as deformation along a line segment that increases in length when a load is applied along that line, however in case of compressive strain this deformation decreases. Ghosh *et.al* illustrated how the changes in lattice strain of nanoparticles is taken place within various crystallite size and within tunable crystal phase of host materials. For instances, it was noticed that nanorods of LaPO<sub>4</sub> doped with Yb and Er had higher tensile strain compared to the nanoparticles. On the other hand, compressive strain was observed for Yb coated LaPO<sub>4</sub> doped with Er nanorods and nanoparticles. In another example, same group further studied the Eu doped LaPO<sub>4</sub> nanocrystal and noticed that tensile and compressive strain were found for the hexagonal and monoclinic phase respectively. In addition, coated nanoparticles have shown compressive nature of strain than the uncoated and rod shaped particles. It means lattice strain is significantly influenced by crystal phase, shape of host material as well as surface coating. Ti-76

Afterwards, the synthesized RE<sup>3+</sup> doped nanoparticles are used for different photonics and bio-photonic applications. For instances, to overcome the limitation (i.e. dimming and utilization of toxic elements like Hg) of conventional white light emitting sources such as compact fluorescent lamps (CFLs) and light emitting diodes (LEDs), now judiciously selected RE ions combinations are being incorporated into the host materials for getting energy efficient white light emitting materials.<sup>48</sup> To achieve this, combination of blue, green

and red light emitting or complimentary color emitting phosphors materials are used such as (1% Eu, 1% Tb, 1% Tm)-co-doped LaF<sub>3</sub> nanoparticles and Dy<sup>3+</sup> and Tm<sup>3+</sup> doped phosphor material, 77-78 β-NaYF<sub>4</sub> nanorods doped with Yb<sup>3+</sup>-Ho<sup>3+</sup>-Tm<sup>3+</sup> and by precisely doping Ce<sup>3+</sup>, Tb<sup>3+</sup> and Eu<sup>3+</sup>/Sm<sup>3+</sup> in suitable host materials may also generate white light.<sup>79</sup> Upconverting phosphors materials are recently incorporated with semiconductors for enhancing the solar cell efficiency. Large extent of loss of solar energy and band gap mismatch are major concerns in semiconductors and organic dyes based solar cell. Therefore, upconverting nanomaterials are incorporated with semiconductor based solar cell for enhancing the solar cell efficiency. 47-48 It is assumed that using the upconverting phosphor materials, Shockley-Queisser efficiency may be enhanced up to ~40% from ~30%.80 For example, Shockley-Queisser efficiency of a 1.7 eV band gap solar cell is enhanced from 28.2% to 33.5–43.6% by upconverting nanoparticles.<sup>81</sup> NaYF<sub>4</sub>:Er<sup>3+</sup> was employed for enhancing NIR silicon solar cell response by Shalav et.al. 82 Furthermore, core-shell hexagonal NaYF<sub>4</sub>:Yb<sup>3+</sup>/Er<sup>3+</sup>@NaYF<sub>4</sub>, core-shell nanostructures of NaYF<sub>4</sub>:Yb<sup>3+</sup>/Er<sup>3+</sup>/Gd<sup>3+</sup> nanorods which is coated with plasmonic Au nanoparticles or Au shells and hexagonal, core-double-shell structured β-NaYF<sub>4</sub>:Er,Yb@SiO<sub>2</sub>@TiO<sub>2</sub> are synthesized for enhancing the solar cell efficiency. 48,83-85 On the other hand, for biological application like photodynamic therapy, sensing the biological species, in vitro-in vivo bio-imaging, nanoparticles must be either water soluble or dispersible. 47-48 However, fluoride-based phosphor nanoparticles are generally less soluble and dispersible in water. 47-48 Therefore, for increasing the solubility and dispersibility, RE<sup>3+</sup> doped nanoparticles are first preliminarily functionalized with biocompatible organic molecules, silica and metallic nanoparticles etc. 47-48 For instance, zinc phthalocyanine (ZnPc) (as photosensitizer) was used for modification of 50 nm-sized PEI (PEI = polyethylimine)/NaYF<sub>4</sub>:Yb<sup>3+</sup>, Er<sup>3+</sup> nanoparticles which generate singlet oxygen upon exciting by 980 nm laser for killing the cancerous cells.<sup>86</sup> Upconverting Er<sup>3+</sup> doped NaYF<sub>4</sub> nanoparticles and modified with gold nanoparticles can also be used for the detection of biological species by FRET-based bio-molecular sensing.<sup>87</sup> Amino-functionalized β-NaYF4:Yb, Er UCNPs have been used as fluorescent probes in cell immunolabelling and imaging. 88 Sub-20 nm sandwich-structured NaGdF<sub>4</sub>:Yb/Tm@NaLuF<sub>4</sub>:Yb/Tm@NaYF<sub>4</sub> nanocrystals were fabricated for in vivo upconversion luminescence and computed tomography imaging.<sup>89</sup> However, to incorporate the magnetic property in the nanomaterial, Fe<sub>3</sub>O<sub>4</sub> nanoparticles were coated with NaLuF<sub>4</sub>:Yb<sup>3+</sup>,Er<sup>3+</sup>/Tm<sup>3+</sup> to form nanocomposites having multipurpose applications like magnetic resonance, charge transfer and upconversion imaging.90

### 1.2.2 Semiconducting luminescent nanomaterials

Another class of luminescent nanomaterial is semiconducting nanomaterials which exhibit completely different optical features than the RE doped luminescent nanomaterials.

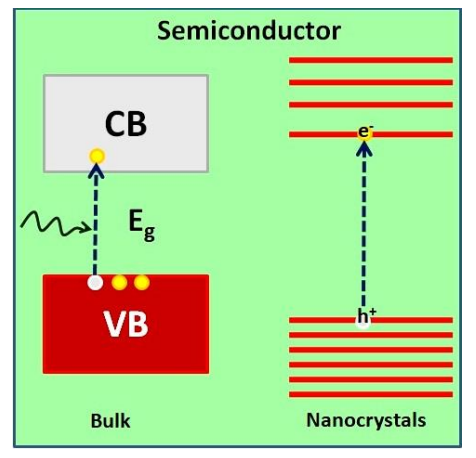


**Figure** 10. Schematic representation of energy levels in bulk and in nanocrystals of semiconductors.

Previously, pure silicon based semiconducting materials were used for the electronic applications for making the transistors and diodes. However, the cost of production of extremely pure elemental silicon is very high. Then silicon is used to be doped with III (Ga) and V (P, AS) group elements for making the p-type and n-type semiconductors respectively. As a result, cost of production and size of the transistors was substantially reduced. Subsequently, inorganic based semiconducting nanoparticles are being used further for miniaturization and reduction of cost production of

transistor and diodes and now are extensively being used for various applications like catalysis, photocatalysis, and photovoltaic, LEDs, solar cell and bio-imaging etc.<sup>24-26,93-96</sup>

Semiconducting nanoparticles have size dependent electronic and optical properties. This size dependent electronic property was first time reported in 1920's. In1980s, Brus and Ekimov illustrated the relation between size of nanocrystallite and their optical properties. <sup>2,24</sup> In 1982, Henglein and Gratzel, used the CdS as catalyst and photosensitizers. <sup>25-26</sup> For rationalizing the relation between particle size with band gap, "particle in one dimensional box" model was used: <sup>2,91</sup>

$$E_g \text{ (eff)} = E_g + \hbar^2 \pi^2 / 2\mu R^2 - 1.8e^2 / \epsilon R$$
 (2)

The term  $E_g$  (eff) is the effective band gap energy,  $E_g$  is bulk band gap energy,  $\hbar^2\pi^2/2\mu R^2$  ( $\hbar=h/2$   $\pi$ ) is due to confinement effect and  $1.8e^2/\epsilon R$  is related to Coulombic interaction energy, and R is the particle radius, and  $\mu=$  reduced mass of electron ( $m_e$ ) and hole ( $m_h$ ) system  $[1/m_e+1/m_h].^{2,24}$ 

Optical and electronic properties are fundamentally originated due to electronic transition between two energy levels i.e. from lower energy valance band (VB) to high energy conduction band (CB), and the gap between these two energy levels is known as band gap

(E<sub>g</sub>) (Figure 10).<sup>2,24</sup> Electronic transition only occurred when the nanoparticles are irradiated with light of either same energy or higher energy than the band gap of semiconducting nanocrystals. As a result, electron and hole are generated. Electron moves to the vacant CB, while hole remains in filled VB. These electron-hole pairs are called exciton. And the size of exciton [also known as Bohr exciton radius (a<sub>B</sub>)] is varied from 1 nm to 100 nm.<sup>2,24</sup> Therefore, on reducing the crystallite size of material from bulk to nanoscale regime, interaction between electron-hole pair increases leading to high energy which is required to separate them. Thereafter, electron and hole recombination is taken place accompanying with radiative emission. On confining the material to nanoscale regime (1-100 nm), intrinsic energy levels of VB and CB are further splitted into discrete energy levels (Figure 10). Generally, in the bulk, electron-hole wave functions are extended to wide region.<sup>2,24</sup> On the other hand, on reducing the crystallite size in the regime of nanosized, these electron-hole wave functions are limited to small volume resulting of increase of columbic interaction and blue shift in absorption energy is noticed. In another word, on decreasing the size of bulk materials to nanoscale, band gap nanoparticles increases and energy levels get more discrete owing to quantum confinement effect. In this way, absorption and fluorescence property is dependent on the size of the nanocrystals.<sup>2,24</sup>

Organic dyes as fluorescent probes were previously used for the detection of biological molecules and studying the biological systems. However, these dyes molecules have inherent limitations such as narrow excitation spectrum, broad emission spectrum with a long tail at red wavelength and less photo-chemical stability. 94,97 For overcoming these issues concerned to the dyes, semiconducting nanoparticles were used which have size dependent, tunable, narrow emission and could be excited in wide range shorter than the emission peak and photo-chemically more stable. 94,97 First time high quality CdSe/ZnS QDs was noticed in 1998 by two independent groups. 94,97 As a result, semiconducting quantum dots were substantially used as fluorescent nanoprobes.<sup>97</sup> Interesting features of these quantum dots are that excitation and emission wavelength can be tuned. Since then, numerous semiconducting quantum dots have been developed for several other applications including photocatalysis, enhancing the solar cell efficiency and bioimaging etc. 97 For example, lanthanide modified CdSe core coated with ZnS shell was synthesized to understand the impact of shell on energy transfer from host to Ln ions and position of Ln ions in the CdSe host (core). 98 On the other hand, Cu<sub>2</sub>S coated CdSe QDs was prepared for increasing their cytoamiability and to augment their specificity towards cancer cells. 99 Ikram modified the TiO2 film using the PbS

QDs to augment the charge transportation at the interface of PbS QDs and TiO<sub>2</sub> film for efficiently generation of PEC hydrogen by water splitting. 100

Owing to improve the luminescence quantum yield, photocatalytic activity, 101 tuning the

fluorescence lifetimes, and dispersibility in water for biological applications, 94,97 tuning the relative bandgap positions of inorganic semiconducting nanomaterials,



surface passivation of core inorganic material with Figure 11. Core-shell structure of other inorganic material as a shell, is the frequently

nanoscale materials

used method to reduce the dangling bond or unsatisfied co-ordination bond. 94,97,102-107 To date, various kinds of materials as a core@shell like structure have been designed for enhancing the aforementioned properties (Figure 11). For instances, CdSe/ZnSe, CdSe/ZnS, Ge/CdS and CdSe/CdS are some of the most promising materials. 105,108-110 Furthermore, plasmonic metal nanoparticles are coated on inorganic semiconducting nanomaterials in core/shell (Au/CdS) heterojunction structures to increase the optical absorption of nanomaterials via energy transfer. 111 On the other hand, to devoid of the toxic elements (Cd, Pb, semiconducting nanomaterials, Hg) consisting other alternative (non-toxic semiconducting nanomaterials) are being looked for designing the core-shell heterojunction structure. For example, Wang et al. synthesized ZnO-Ag<sub>2</sub>S core-shell structure for enhancing the field emission properties of ZnO nanowires using the successive ionic layer adsorption and reaction (SILAR) approach, in which Ag<sub>2</sub>S is employed for making the shell about the ZnO nanowires, which has negligible toxicity. 112

### 1.2.2.1 Metal ion doped semiconducting nanomaterials

Doping of transition metal ions and rare-earth ions in semiconducting nanoparticles or quantum dots also substantially increases the luminescence property for several applications from solar cell to bio-imaging. 113 For instances, Liu et al. tuned the PL emission of CdS QDs ranging from visible to NIR region (590-800 nm) and fluorescence quantum yield is noticed up to 40% through doping of In and Cu. 114 However, solid state semiconductor, with efficient light emitting CuCdS NCs with high PLQY (approximately 55%) was found by Acharya and co-workers. 115 Cao et al. synthesized Cu-doped Zn-In-Se ternary chalcogenide quantum dots (QDs). Due to large Stokes shift and composition (Zn/In ratio) based tunable photoluminescence (PL), emission features from visible to near-infrared (NIR) (ca. 565–710 nm) spectral range. 116 PL quantum yield (QY) of the Cu doped ternary QDs was noticed up to 38% after coating with ZnSe shells. 116 To increase the deep tissue imaging and as cellular nanoprobes having near-infrared persistent luminescence, 5-nm ZnSn<sub>2</sub>O<sub>4</sub> (ZSO) ultra small nanoparticles are doped with Cr and Eu which exhibit NIR afterglow emission at 800 nm. ZSO was also conjugated with folic acid for increasing the tumor targeting capacity under *in vitro* and *in vivo* conditions.<sup>117</sup> Shen *et al.* prepared the Ag<sub>2</sub>S-ZnS heteronanostructures (HNSs) doped with Mn and found that multicolor emissions are occurring in blue, orange, and near-infrared (NIR) region owing to the presence of various emission sites in the HNSs.<sup>118</sup> On the other hand, due to presence of oxygen vacancies and doping of Mn in ZnO microflowers, intense luminescence as well as water splitting in visible region is observed.<sup>119</sup> Ho *et al.* incorporated the Nb in the nontoxic beta-In<sub>2</sub>S<sub>3</sub> at different concentration for enhancing its photoelectric-conversion yield.<sup>120</sup>

### 1.2.2.2 Metal and semiconducting plasmonic nanomaterials

In addition of excitonic property which is the basic feature of semiconductors, <sup>121</sup> copper chalcogenides (Cu<sub>2</sub>X, X=S, Se, Te) and copper phosphide etc. have dual mode of optical behaviors <sup>121</sup> These nanoparticles also have the plasmonic property which is inherently occurred in metallic nanoparticles especially gold (Au), silver (Ag), copper (Cu) etc.. <sup>122-128</sup> This plasmonic behavior which is occurring in copper chalcogenides can be attributed to collective oscillation of holes, which is just contrary to metal based plasmonic nanoparticles in which surface bound free electrons are responsible. <sup>129-130</sup> These oscillated holes are induced via oxidation which leads to the generation of Cu vacancies. These optical characteristics and metal based plasmonic nanoparticles are considered as good candidate for wide range of applications including light harvesting, nonlinear optics, bio-imaging, and quantum information processing. <sup>129-130</sup>

### 1.2.3 Graphene oxide Nanocomposite Luminescent Nanomaterials

In last few decades, numerous forms of carbon based materials have been discovered which are found in different shape and size including 3D graphite to 1D carbon nanotubes such as single-walled carbon nanotube (SWNT) and multiwalled carbon nanotube (MWNT) (shown in **Figure 12a-f**). Graphene is two dimensional (2D) (Figure 12b), one atom thick with sp<sup>2</sup> hybridized carbon, having zero band gap, and honey comb like structure. In addition, it possess fascinating electrical, mechanical, thermal and optical properties.<sup>131</sup> For instances, it has very high mobility of charge carriers at room temperature (200 000 cm<sup>2</sup> V<sup>-1</sup> s<sup>-1</sup>), fracture strength (125 GPa),<sup>2</sup> Young's modulus (~1100 GPa),<sup>2</sup> thermal conductivity (~5000 W m<sup>-1</sup> K<sup>-1</sup>), specific surface area (theoretical value of 2630 m<sup>2</sup> g<sup>-1</sup>), and high optical transmittance.<sup>131</sup>

Consequently, it is significantly paving a way for several applications concerned with energy storage and conversion devices. The exploration of this fantastic material is not very old. Before 2004, it was believed that thermodynamically two-dimensional crystal could not exist in many omnibuses of experimental observations. <sup>133-134</sup> By breaking this idea, Novoselov *et al.* separated the graphene by micromechanical cleavage technique from the graphite in 2004. <sup>30</sup> Now it can be synthesized using the soft chemical methods. <sup>131</sup>

From the point of view of optical applications, opening of its band gap is very important task. This can be done either by donating or withdrawing the free electrons. To achieve this, numerous practices such as chemical functionalization with organic groups, doping with heteroatoms like N, B, P, S, O etc. formation of nanocomposite with graphene surface and reducing its size to zero dimensions are frequently being used. Chemically functionalized graphene

is known as graphene oxide (GO), in which graphene is highly decorated with organic moieties like hydroxyl (-OH), epoxy (C-O-

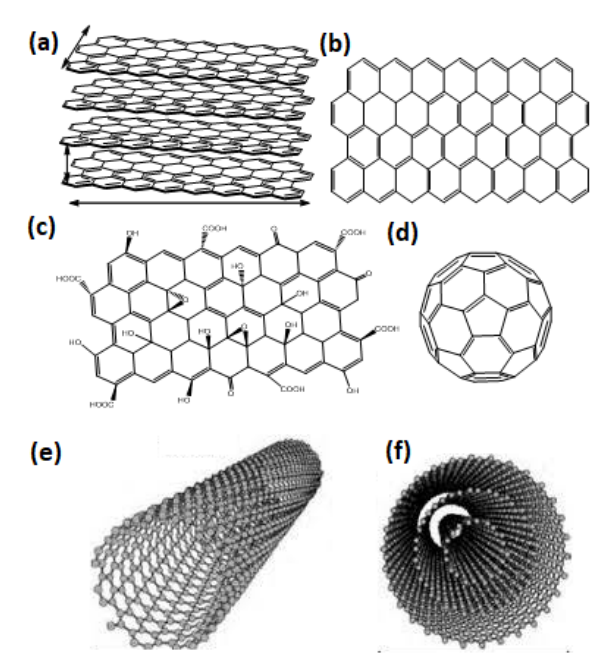


**Figure 12.** Types of carbon-based nano structures: a) graphite, b) graphene, c) graphene oxide, d) fullerene, e) SWNT and f) MWNT

C), ketonic (-C=O) and carboxyl (-COOH) groups. It is established that on functionalization of graphene with organic group and inorganic materials also leads to opening of band gap. <sup>131</sup> Another important feature of graphene oxide is that it also shows the size dependent optical behavior, on confining it to 0D (zero dimension) which is also known as graphene quantum dots. On exciting these QDs at suitable wavelength, it shows blue or green emission. However, the partly reduced GO using the different reducing agents or method are called reduced graphene oxides (RGO). Furthermore, other inorganic semiconducting, metallic, rare-earth ions, rare-earth doped nanocrystals and quantum dots including CdS, CdSe, ZnO, In<sub>2</sub>S<sub>3</sub>, Ag, Au, Pt, Yb and Er doped NaYF<sub>4</sub> and so on, are decorated onto the surface of graphene oxide for various applications such as photocatalysis, catalysis, solar cell application, photovoltaic, as sensors and optical materials. <sup>136</sup>

Singh et al. prepared the ZnO decorated on luminescent graphene sheets using single step synthesis method for the detection of common industrial toxic gases like CO, NH<sub>3</sub> and NO at very low concentration up to 1 ppm at room temperature. 137 Opto-electronic properties of semiconducting ZnO-graphene oxide is also studied in which emission is blue shifted as well as quenched in the presence of GO.<sup>137</sup> Luminescence quenching of green emitted ZnO in the presence of GO has also been illustrated by William et al., in which electron is transported from ZnO to graphene oxide for reduction to graphene as well as increasing the electrical conductivity. 138 Hierarchical ZnO hollow sphere has been decorated onto the GO for increasing the photocurrent and photodegradation efficiency of methylene as compared to bare ZnO. 139 It was found that in the presence of GO, electron lifetime increases and suppression of electron hole recombination is also occurred. Photo-conversion efficiency (PCE) of solar cells has been enhanced using the electrodeposited ZnO nanorods on reduced graphene oxide (rGO). <sup>140</sup> Ajayan and co-workers prepared novel electroluminescent device in which new phosphor material is designed by Cu/Al doped ZnS as active emitter layer wrapped with rGO (for enhancing the local current) and exfoliated BN is used as dielectric laver. 141 Nanocomposite of reduced GO decorated with ZnS/CuS nanospheres is synthesized using solvothermal method combined with cation exchange process. <sup>142</sup> It is seen that the photocatalytic degradation efficiency is improved up to 99.22% which is higher than that of bare ZnS and ZnS/CuS nanosphere. 142 Cactus and honeycomb like ZnSe microspheres of size 10µm and 6µm respectively have been successfully decorated on the graphene oxide sheet using the hydrothermal method. PL spectra of this ZnSe/Graphene oxide microsphere show that blue-green light emission is occurring upon exciting by UV source. 143 Lin et al. synthesized CdSe-rGO nanocomposite by decorating CdSe nanoparticles onto rGO through a linker free mechanism. 144 They found that this nanocomposite has improved photoresponse feature compared to the individual CdSe and rGO. However, photoluminescence of CdSe nanoparticles is immensely quenched in the presence of rGO.<sup>144</sup>

### References

- 1 E. V. Shevchenko and Dmitri V. Talapin, Chem. Rev. 2016, 116, 10343.
- 2 L. E. Brus, J. Chem. Phys. 1984, **80**, 4403.
- 3 D. L. Leslie-Pelecky, *Chem. Mater.* 1996, **8**, 1770\.
- 4 K. Ariga, M. Li, G. J. Richards, and J. P. Hill. J. Nanosci. Nanotechnol. 2011, 11,1.
- **5** C. Bai and M. Liu, *Angew. Chem. Int. Ed.* 2013, **52**, 2678.
- **6** F. C. Adams and C. Barbante, *Spectrochimica Acta Part B*, 2013, **86**, 3.

- 7 T. Takagahara and K. Takeda, *Physical Review B*, 1992, **46**, 15578.
- 8 D. Kim, N. Lee, Y. I. Park and T. Hyeon, *Bioconjugate Chem.*, 2017, 28, 115.
- 9 A.Albanese, P. S. Tang, and W. C.W. Chan, Annu. Rev. Biomed. Eng. 2012, 14, 1.
- 10 M. Cardon, The Devil and the Surfaces, 2006.38.
- 11 E. Roduner, Chem. Soc. Rev., 2006, 35, 583.
- **12** N. G. Khlebtsov, L. A. Dykman, *Journal of Quantitative Spectroscopy & Radiative Transfer*, 2010, **111**, 1.
- 13 I. Chakraborty and T. Pradeep. Chem. Rev. 2017, 117, 8208.
- **14** M. Faraday, *Philosophical Transactions of the Royal Society of London*, 1847, **147**, 159.
- **15** S. Eustis and M. A. El-Sayed, *Chem. Soc. Rev.*, 2006, **35**, 209.
- 16 M-C. Daniel and D. Astruc, Chem. Rev. 2004, 104, 293.
- 17 M. Yang and H. Papp, Chin.J. Chem. Phys. 2007, 20, 690.
- **18** Y. Nakae, Y. Seino, T. Teranishi, M. Miyake, S. Yamada and H. Hori, *Physica B*, 2000, **1758**, 284.
- **19** Y. Yamamoto, T. Miura, Y. Nakae, T. Teranishi, M. Miyake and H. Hori, *Physica B*, 2003, **1183**, 329.
- 20 E. Abbasi, M. Milani, S. F. Aval, M. Kouhi, A. Akbarzadeh, H. T. Nasrabadi, P. Nikasa, S. W. Joo, Y. Hanifehpour, K. Nejati-Koshki, and M. Samiei, *Crit Rev Microbiol*, 2016, 42, 173.
- **21** R. Zsigmondy, Colloids and the Ultramicroscope, chapters IV and V, John Wiley & Sons, Inc., New York, 1914
- 22 R.P. Feynman, *Eng. Sci.* 1960, 23, 22.
- 23 N. Taniguchi, "Proc. Intl. Conf. Prod. Eng. Tokyo, Part II, Japan Society of Precision Engineering, 1974.
- 24 M. Nirmal, L.E. Brus, Science 1996, 271, 933.
- 25 A. Henglein, Chem. Rev. 1989, 89, 1861.
- **26** M. Gratzel, *Curr. Opin. Colloid* 1999, **4**, 314.
- **27** H.W. Kroto, J. R. Heath, S. C. O'Brien, R. F. Curl, R. E. Smalley, *Nature* 1985, **318**, 162.
- 28 S. Iijima, *Nature* 1991, 354, 56.
- **29** D. S. Bethune, C. H. Klang, M. S. de Vries, G. Gorman, R. Savoy, J. Vazquez and R. Beyers, *Nature* 1993, **363**, 605-607.

- Novoselov, K. S. *et al.* Electric field effect in atomically thin carbon films. *Science* 2004, **306**, 666.
- Gusev A. I. Nanomaterials, Nanostructures, and Nanotechnologies (in Russian) // Fizmatlit, Moscow (2007) 416 pp;
- Gusev A. I., Rempel A. A. *Nanocrystalline Materials. Cambridge: Cambridge International Science Publishing*, 2004. 351 p.
- 33 S. Shionoya, J. Lumin. 1970, 12, 17.
- B. Valeur and M. N. Berberan-Santos. *J. Chem. Educ.* 2011, **88**, 731.
- Braslavsky, S. E. et al.; Glossary of Terms used in Photochemistry, 3rd edition (IUPAC recommendations 2006), *Pure Appl. Chem.* 2007, **79**, 293465.
- B. R. Branchini, Chemistry of Firefly Bioluminescence, Department of Chemistry, Connecticut College New London, CT 06320 brbra@conncoll.edu and Google images.
- J. W. Hastings, Bioluminescence. In Cell Physiology Source Book (Sperelakis, N., Ed.) 1995, pp 665, Academic Press, New York.
- E. H. White, E. Rapaport, H. H. Seliger, and T. A. Hopkins, *Bioorganic Chemistry* 1971, **1**, 92.
- J.-F. Rees, B. De Wergifosse, O. Noiset, M. Dubuisson, B. Janssens and E. M. Thompson, *J. Exp. Biol.* 1998, **201**, 1211.
- 40 T. Goto Marine Natural Products, 2012 books.google.com
- 41 https://www.hakaimagazine.com/features/secret-history-bioluminescence/
- https://www.treehugger.com/natural-sciences/nature-blows-my-mind-8-brilliant-bioluminescent-creatures.html;
- 43 http://www.fireflyexperience.org/photos/
- https://northofthegrid.com/2016/05/16/arctic-facts-bio-luminescent-glow-in-the-dark-zooplankton-during-the-arctic-night/
- 45 http://squid.tepapa.govt.nz/the-deep/article/bioluminescence-in-the-deep-ocean;
- 46 https://www.flickr.com/photos/nickadel/15822210628/sizes/h/
- 47 S. Gai, C. Li, C. Yang, P. Yang and J. Lin, Chem. Rev. 2013, 114, 2343.,
- R. K. Sharma, A-V. Mudring and P.Ghosh, *J. Lumin.* 2017, **189**, 44.
- S.-V. Eliseeva and J.-C. Bünzli, *Chem. Soc. Rev.* 2010, **39**, 189.
- J.-C. Bünzli, *Chem. Rev.* 2010, **110**, 2729.
- 51 F. Auzel, Chem. Rev. 2004, 104, 139.
- V. Ovsyankin, P.P. Feofilov, *JETP Lett.* 1966, **3**, 317.

- **53** J.C. Boyer and F.C.J.M. van Veggel, *Nanoscale*, 2010, **2**, 1417.
- **54** P. Ghosh, A. Kar and A. Patra, *Nanoscale*, 2010, **2**, 1196.
- **55** H. Dong, L.-D. Sun and C.-H. Yan, *Chem. Soc. Rev.*, 2015, **44**, 1608.
- 56 X. Chen, D. Peng, Q. Ju and F. Wang, Chem. Soc. Rev., 2015, 44, 1318.
- **57** C. Lorbeer and A.-V. Mudring, *Chem. Commun.* 2014, **50**, 13282.
- 58 C. Lorbeer, F. Behrends, J. Cybinska, H. Eckert and A.-V. Mudring, *J. Mater. Chem.* C 2014, 2, 9439.
- **59** C. Lorbeer, J. Cybinska and A.-V. Mudring, *J. Mater. Chem. C*, 2014, **2**, 1862.
- **60** P. Ghosh, S. Tang and A.-V. Mudring, *J. Mater. Chem.*, 2011, **21**, 8640.
- **61** F.Auzel, C. R Acad.Sci.(Paris) 1966, **262**,1016.
- **62** F. Wang, R. Deng, J.Wang, Q.Wang, Y. Han, H. Zhu, X. Chen and X. Liu, *Nat. Mater.*, 2011, **10**, 968.
- **63** M. Wang, Q.-L. Huang, H.-X. Zhong, X.-T. Chen, Z.-L. Xue and X.-Z. You, *Cryst. Growth Des.* 2007, **7**, 2106.
- 64 J. Shan and Y. Ju, Appl. Phys. Lett. 2007, 91, 123103
- 65 P. Ghosh and A. Patra, J. Phys. Chem. C 2008, 112, 19283
- 66 J. Zhung, J. Wang, X. Yang, I.D. Williams, W. Zhang, Q. Zhang, Z. Feng, Z. Yang,C. Liang, M. Wu and Q. Su, *Chem. Mater.* 2009, 21, 160.
- 67 J. W. Stouwdam and F. C. J. M. van Veggel, Langmuir 2004, 20, 11763
- **68** K. Ko"mpe, H. Borchert, J. Storz, A. Lobo, S. Adam, T. Möller, M. Haase, *Angew. Chem.*, *Int. Ed.* 2003, **42**, 5513
- **69** G.-S. Yi and G.-M. Chow, *Chem. Mater.* 2007, **19**, 341
- 70 L. Zhu, Q. Li, X. Liu, J. Li, Y. Zhang, J. Meng and X. Cao, J. Phys. Chem. C 2007, 111, 5898.
- 71 H.-X. Mai, Y.-W. Zhang, R. Si, Z.-G. Yan, L.-D. Sun, L.-P. You and C.-H. Yan, *J. Am. Chem. Soc.*, 2006, **128**, 6426
- **72** M. Wang, Q.-L. Huang, J.-M. Hong, X.-T. Chen and Z.-L. Xue, *Cryst. Growth Des*, 2006, **6**, 1972
- **73** X. Yu, W. Bian, T. Wang, D. Zhou, J. Qiu and X. Xu, *CrystEngCommun.*, 2015, **17**, 2147.
- 74 K. G. Williamson and H. W. Hall, Acta Metall. 1953, 1, 32.
- 75 P. Ghosh, J. Oliva, E. De la Rosa, K. K. Haldar, D. Solis and A. Patra, *J. Phys. Chem. C*, 2008, **112**, 9650.
- **76** P. Ghosh, A. Kar and A. Patra, *J. Appl. Phys.*, 2010, **108**, 113506.

- 77 C. Lorbeer and A.-V. Mudring, J. Phys. Chem. C, 2013, 117, 12229.
- C. Lorbeer and A.-V. Mudring, *ChemSusChem*, 2013, **6**, 2382.
- L.W. Yang, H.L. Han, Y.Y. Zhang and J. X. Zhong, *J. Phys. Chem. C* 2009, **113**, 18995.
- T. Trupke, A. Shalav, B. S. Richards, P. Wurfel, M. A. Green, *Sol. Energy Mater. Sol. Cells*, 2006, **90**, 3327.
- G. Chen, H. Ågren, T.Y. Ohulchanskyy and P.N. Prasad, *Chem. Soc. Rev.* 2015, **44**, 1680.
- A. Shalav, B. S. Richards, T. Truppe, K.W. Krämer and H.U. Güdel, *Appl. Phys. Lett.* 2005, **86**, 013505.
- 83 X. Li, F. Zhang and D. Zhao, Chem. Soc. Rev., 2015, 44, 1346.
- Z. Q. Li, X.D. Li, Q.Q. Liu, X.H. Chen, Z. Sun, C. Liu, X. J. Ye and S. M. Huang, *Nanotechnology*, 2012, **23**, 025402.
- N. M. Idris, M.K.G. Jayakumar and A. Bansal, Y. Zhang, *Chem. Soc. Rev.* 2015, **44**, 1449.
- D. K. Chatterjee and Z. Yong, *Nanomedicine* 2008, **3**, 73.
- P. Zhang, S. Rogelj, K. Nguyen and D. Wheeler, *J. Am. Chem. Soc.* 2006, **128**, 12410-12411.
- M. Wang, C.-C. Mi, W.-X. Wang, C.-H. Liu, Y.-F. Wu, Z.-R. Xu, C.-B. Mao and S.-K. Xu, *ACS Nano*, 2009, **3**, 1580-1586.
- 89 J.W. Shen, J. Wang, D. Kong and X. P. Yan, *RSC Adv.*, 2014, 4, 5088.
- X. Zhu, J. Zhou, M. Chen, M. Shi, W. Feng and F. Li, *Biomaterials*, 2012, **33**, 4618-4627.
- R. W. Keyes, *Rep. Prog. Phys.* 2005, **68**, 2701–2746.
- 92 F.A. Ponce and D. P. Bour, *Nature*, 1997, 386, 351.
- N. Manyala1, Y. Sidis, J. F. Ditusa, G. Aeppli, D. P. Young and Z. Fisk, *Nat. Mater.*, 2004, **3**, 255.
- M. Bruchez Jr, M. Moronne, P. Gin, S. Weiss and A. P. Alivisatos, *Science*, 1998, **281**, 2013.
- 95 A. M. Smith and S. Nie, Acc. Chem. Res., 2010, 43, 190.
- 96 L. Liu, Q. Peng, Y. Li, *Inorg. Chem.* 2008, 47, 5022.
- 97 W. C. Chan and S. Nie, Science, 1998, 281, 2016–2018.
- J. R. Dethlefsen, A. A. Mikhailovsky, P. T. Burks, A. Døssing and P. C. Ford, *J. Phys. Chem. C*, 2012, **116**, 23713.

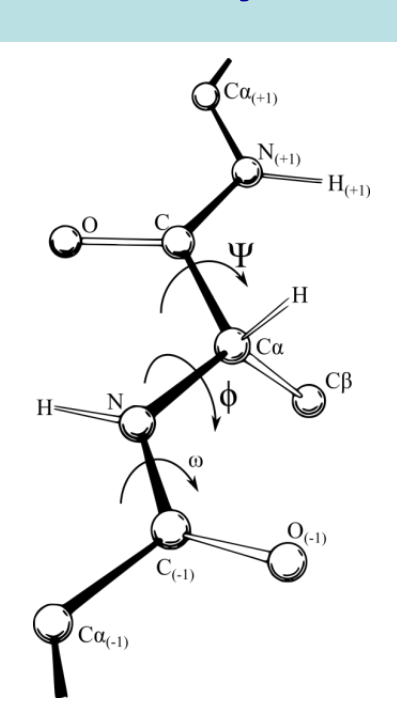
- 99 M. S. Mohamed, A. C. Poulose, S. Veeranarayanan, R. R. Aburto, T. Mitcham, Y. Suzuki, Y. Sakamoto, P. M. Ajayan, R. R. Bouchard, Y. Yoshida, T. Maekawaa and D. S. Kumar, *Nanoscale*, 2016, 8, 7876.
- **100** A. Ikram, S. Sahai, S. Rai, S. Dass, R. Shrivastav and V. R. Satsangi, *Phys. Chem. Chem. Phys.*, 2016, **18**, 15815-15821.
- **101** S. Khanchandani, S. Kundu and A. Patra and Ashok K. Ganguli, *J. Phys. Chem. C*, 2012, **116**, 23653.
- 102 L. Spanhel, M. Haase, H. Weller, A. Henglein, J. Am. Chem. Soc. 1987, 109, 5649.
- 103 D. J. Norris, A. Sacra, C. B. Murray, M. G. Bawendi, M. G. *Phys. Rev. Lett.* 1994,72, 2612.
- 104 W. Hoheisel, V. L. Colvin, C. S. Johnson, A. P. Alivisatos, *J. Chem. Phys.* 1994,101, 8455.
- 105 M. Danek, K. F. Jensen, C. B. Murray, M. G. Bawendi, M. G. *Chem. Mater.* 1996, 8, 173.
- **106** M. A. Hines and P. Guyot-Sionnest. J. Phys. Chem., 1996, **100**, 468.
- 107 M. Danek, K. F. Jensen, C. B. Murray, M. G. Bawendi, M. G. Appl. Phys. Lett. 1994, 65, 2795.
- 108 A. R. Kortan, R. Hull, R. L. Opila, M. G. Bawendi, M. L. Steigerwald, P. J. Carroll, L. E. Brus, *J. Am. Chem. Soc.* 1990, 112, 1327-1332.
- **109** Z. Sun, Z. Shao, X. Wu, T. Jiang, N. Zheng and J. Jie, *CrystEngComm*, 2016, **18**, 3919-.
- **110** Y. Tian, T. Newton, N. A. Kotov, D. M. Guldi and J. H. Fendler, *J. Phys. Chem.*, 1996, **100**, 8927.
- 111 S. Lambright, E. Butaeva, N. Razgoniaeva, T. Hopkins, B. Smith, Di. Perera, J. Corbin, E. Khon, R. Thomas, P. Moroz, A. Mereshchenko, A. Tarnovsky, and M. Zamkov, ACS Nano, 2014, 8, 352.
- 112 G. Wang, M. Li, C. Chen, S. Lv, J. Liao and Z. Li, Dalton Trans., 2016, 45, 8777.
- **113** K. E. Knowles, K. H. Hartstein, T. B. Kilburn, A. Marchioro, H. D. Nelson, P. J. Whitham and D. R. Gamelin, *Chem. Rev.* 2016, **116**, 10820.
- **114** M. Liu, W. Yao, C. Li, Z. Wu and L. Li, *RSC Adv.*, 2015, **5**, 628.
- **115** A. H. Khan, A. Dalui, S. Mukherjee, C. U. Segre, D. D. Sarma and S. Acharya, *Angew. Chem. Int. Ed.*, 2015, **54**, 2643.
- **116** S. Cao, W. Ji,c J. Zhao, W. Yang, C. Li and J. Zheng, *J. Mater. Chem. C*, 2016, **4**, 581.

- J.-L. Li, J.-P. Shi, C. Wang, P.-H. Li, Z.-F. Yu and H.-W. Zhang. *Nanoscale*, 2017, **9**, 8631.
- S. Shen, Y. Zhang, Y. Liu, L. Peng, X. Chen and Q. Wang, *Chem. Mater.* 2012, **24**, 2407.
- B. Sambandam, R. J. V. Michael and P. T. Manoharan, *Nanoscale*, 2015,**7**, 13935-13942
- 120 C.-H. Ho, J. Mater. Chem., 2011, 21, 10518.
- P. L. Saldanh, R. Brescia, M. Prato, H. Li, M. Povia, L. Manna, and V. Lesnyak, *Chem. Mater.* 2014, **26**, 1442.
- Y. Zhao, H. Pan, Y. Lou, X. Qiu, J. Zhu, C. Burda. *J. Am. Chem. Soc.* 2009, **131**, 4253.
- **123** Y. Xie, L. Carbone, C. Nobile, V. Grillo, S. D'Agostino, F. Della Sala, C. Giannini, D. Altamura, C. Oelsner, C. Kryschi, P. D. Cozzoli, *ACS Nano*, 2013, **7**, 7352.
- Y. Xie, A. Riedinger, M. Prato, A. Casu, A. Genovese, P. Guardia, S. Sottini, C. Sangregorio, K. Miszta, S. Ghosh, T. Pellegrino, L. Manna. *J. Am. Chem. Soc.* 2013, **135**, 17630.
- Kriegel, C. Jiang, J. Rodríguez-Fernández, R. D. Schaller, D. V. Talapin, E. da Como, J. Feldmann, *J. Am. Chem. Soc.* 2012, **134**,1583.
- B. I. Ipe, K. Yoosaf, and K. G. Thomas, *J. Am. Chem. Soc.*, 2006, **128**, 1907.
- C. Hamon, M. N. Sanz-Ortiz, E. Modin, E. Hill, L. Scarabelli, A. Chuvilin and L. M. Liz-Marzan *Nanoscale*, 2016, **8**, 7914.
- K. W. Choi, S. W. Kang, D. Y. Kim, S. H. Im, Y. Park, S. W. Han and O O. Park, *J. Mater. Chem. C*, 2016, **4**, 3149.
- P. D. Cozzoli, T. Pellegrino, L. Manna, *Chem. Soc. Rev.* 2006, **35**, 1195.
- 130 C. d. M. Donega, Chem. Soc. Rev. 2011, 40, 1512.
- V. Georgakilas, J. N. Tiwari, K. C. Kemp, J. A. Perman, A. B. Bourlinos, K. S. Kim, and R. Zboril, *Chem. Rev.* 2016, **116**, 5464.
- G. Zhao, T. Wen, C. Chen and X. Wang, *RSC Advances*, 2012, **2**, 9286.
- Peierls, R. E. Quelques proprietes typiques des corpses solides. *Ann. I. H. Poincare* 1935, **5**, 177.
- Landau, L. D. Zur Theorie der phasenumwandlungen II. *Phys. Z. Sowjetunion*, 1937, **11**, 26.
- X. Wang, G. Sun, P. Routh, D.-H. Kim, W. Huang and P. Chen, *Chem. Soc. Rev.*, 2014, **43**, 7067.

- 136 N. Gao and X. Fang, Chem. Rev., 2015, 115, 8294.
- **137** G. Singh, A. Choudhary, D. Haranath, A. G. Joshi, N. Singh, S. Singh, R. Pasricha, *CARBON*, 2012, **50**, 385.
- 138 G. Williams and P. V. Kamat, *Langmuir*, 2009, 25, 13869.
- **139** Q-P. Luo, X-Y. Yu, B-X. Lei, H-Y. Chen, D-B. Kuang and C-Y. Su, *J. Phys. Chem. C* 2012, **116**, 8111.
- **140** Z. Yin, S. Wu, X. Zhou, X. Huang, Q. Zhang, F. Boey, and H. Zhang, *small* 2010, **6**, 307.
- 141 B. K. Gupta, S. Singh, G. Kedawat, K. Nagpal, P. Kumar, A. K. Gangwar, T. N. Narayanan, A. A. Marti, R. Vajtai and P. M. Ajayan Nanoscale, 2017, 9, 5002.
- 142 L. Yang, X. Guan, G-S. Wang, X-H. Guan and B. Jiad, New J. Chem., 2017, 41, 5732.
- **143** J. Han, S. Xue, W. Zhou, S. Wu, P. Xie, R. Zou, *J. Colloid and Interface Sci.*, 2014, **430**,116.
- Y. Lin, K. Zhang, W. Chen, Y. Liu, Z. Geng, J. Zeng, N. Pan, L. Yan, X. Wang, and J. G. Hou, *ACS Nano*, 2010, **4**, 3033.

# Ramchandran Diagram (M.Sc II Semester, CHE-CC-224)







# Dr. Pushpal GHOSH

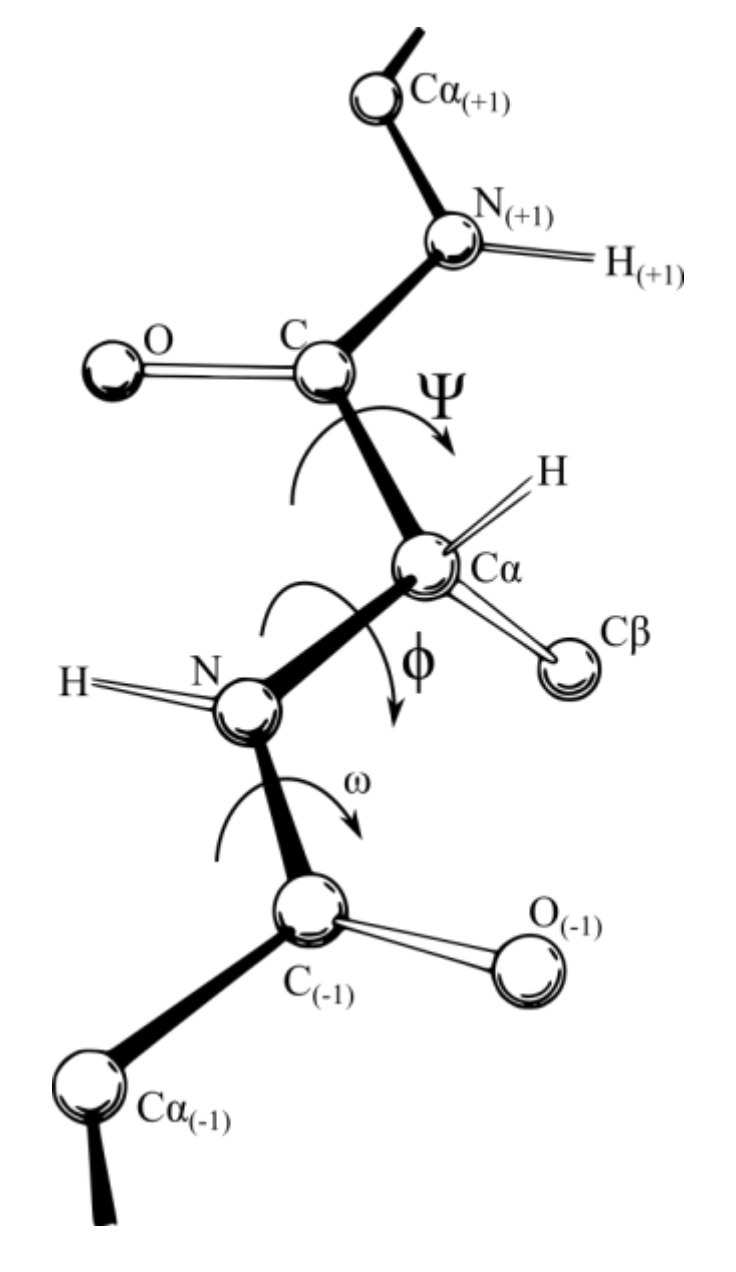
Assistant Professor (Alexander von Humboldt Fellow)

Department of Chemistry,

Dr. Harisingh Gour Vishwavidyalaya (A Central University),

 Ramachandran diagram, originally developed in 1983 by G.N.Ramachandran, C.Ramakrishnan and V.Sasisekharan is a way to visualise backbone dihedral angles  $\psi$  against  $\emptyset$  of amino acid residues in protein structure. A protein chain is made up of a large number of different amino acids linked in a sequential way through amide/peptide linkages. The basic system that was used formulation in the Ramachandran map is a system of two trans -planar peptide units

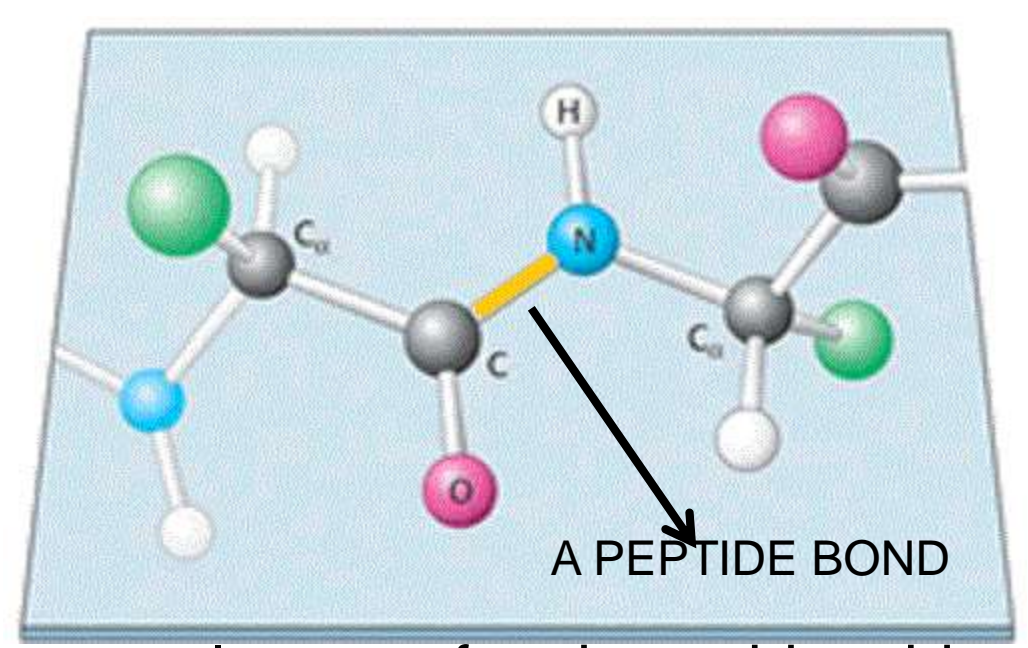
linked at the central α atom.



# Why we plot Ramchandran diagram

The purpose of Ramchandran plot is to show as the sterically permissible configuration of amino acid dihedral angles allowed with in biological protein.

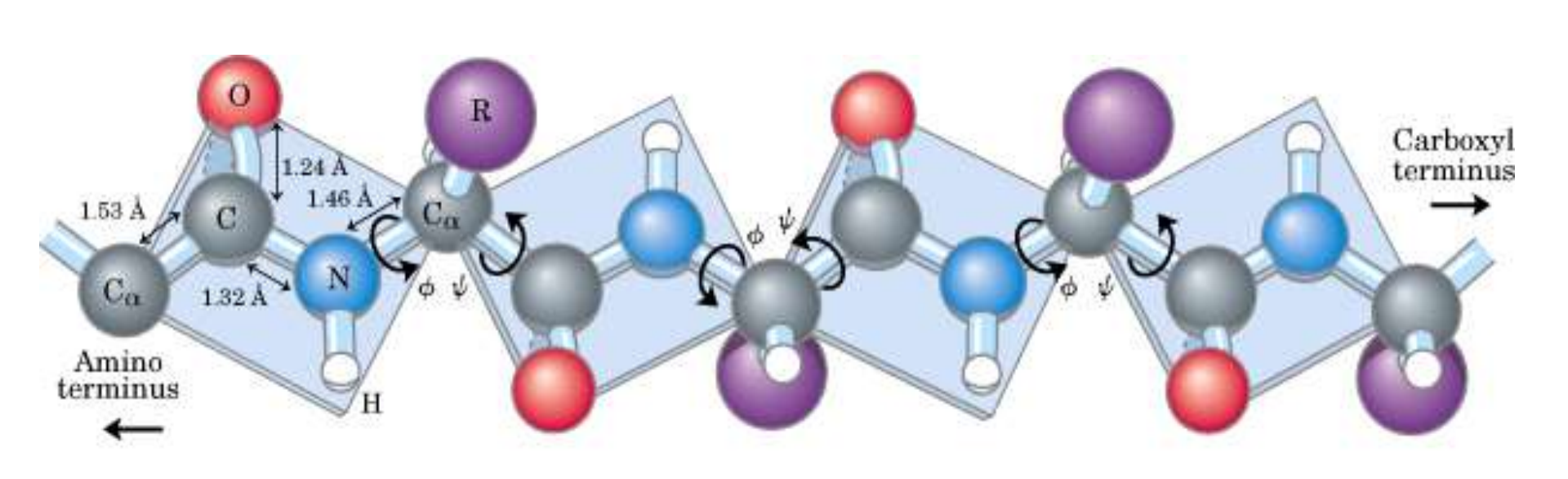
## A PEPTIDE BOND



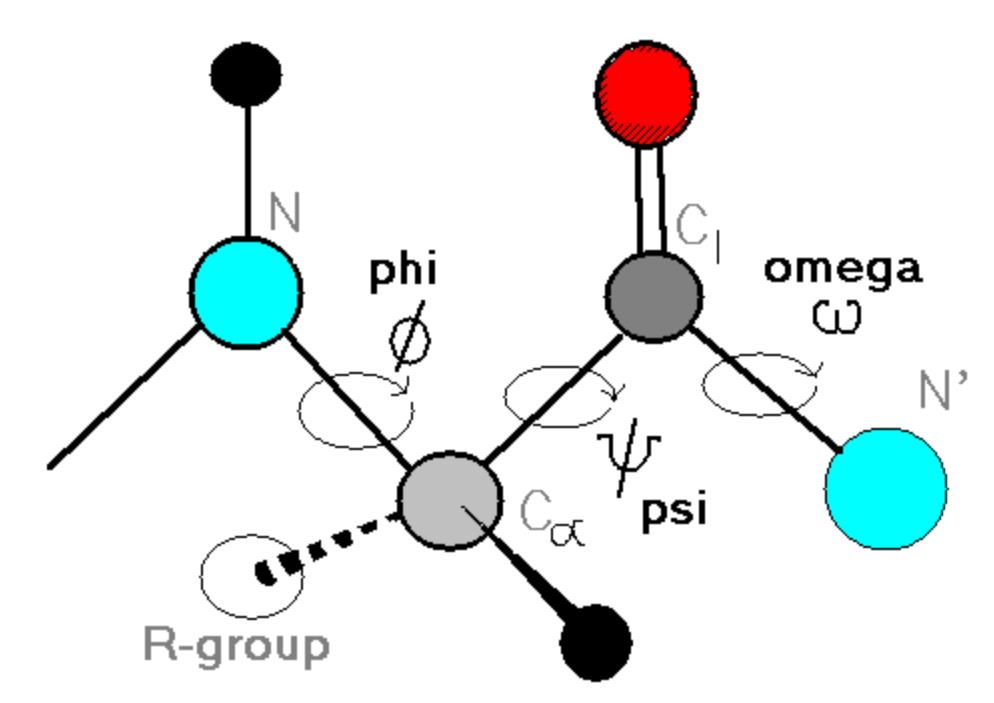
- •Polypeptides are polymers of amino acid residues linked by peptide group
- Peptide group is planar in nature which limits the conformational flexibility of polypeptide chain

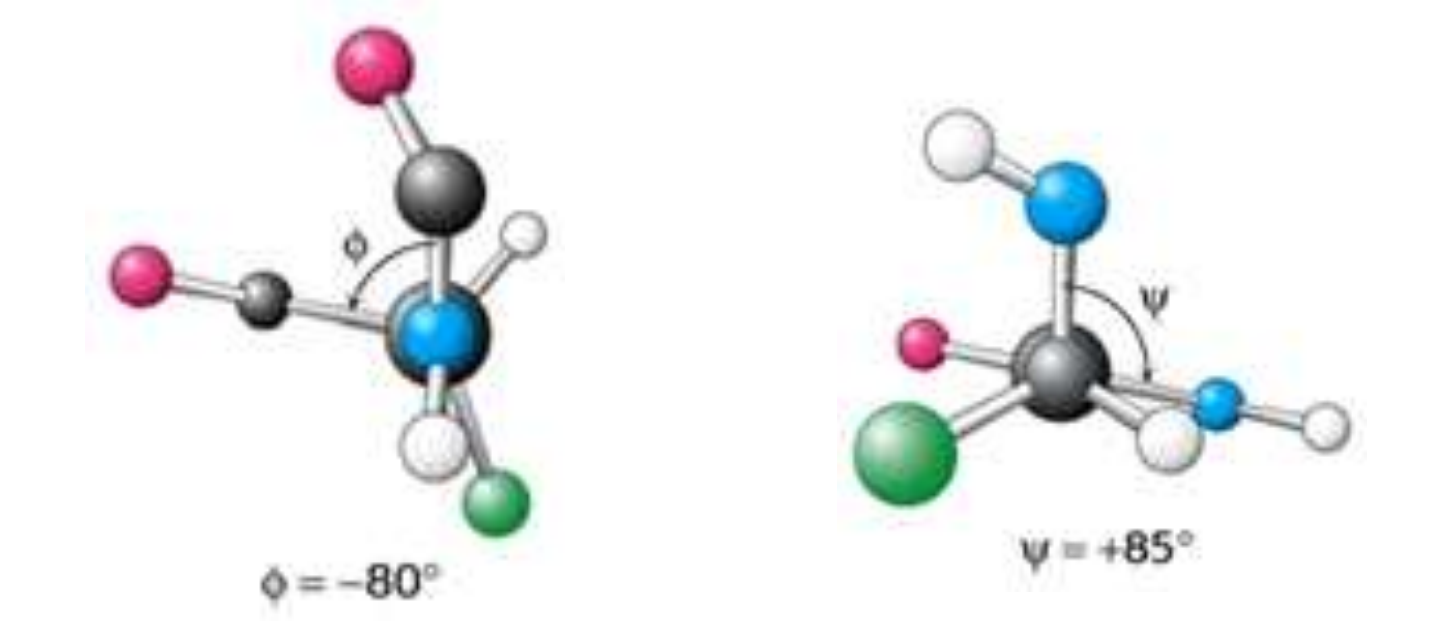
- •Structure of peptide group was analysed by Linus Pauling and Robert Corey in 1930 s.
- •They performed x-ray diffraction studies of crystals of amino acids and simple di and tri peptides.
- Study showed that
- O=C—N peptide bond is shorter than O=C—N bond in simple amines
- > Atoms associated with peptide bonds are coplanar
- ➤ A small electric dipole is formed by resonance or partial sharing of two pairs of electrons between the carbonyl oxygen and amide nitrogen
- The six atoms of peptide group lie in a single plane with O of C=O and H of NH being trans to each other

# **TORSION ANGLES**



- ■The backbone or main chain of a polypeptide involves the atoms in peptide bond i.e., a linked sequence of rigid planar peptide groups with consecutive planes sharing a common point of rotation at Ca
- •The conformation of this backbone is described by torsion angles / dihedral angles / rotational angles around Ca –N ( $\phi$ ) bond and Ca --C ( $\psi$ ) bond of each residue





The angles and are both 180 when the polypeptide chain is in its fully extended conformation and all peptide groups are in same plane

In principle, both these angles can have any values between +180 and - 180, but many values are sterically constrained.

ie., rotation around  $C_\alpha$ —N and C— $C_\alpha$  bonds forming certain a  $\psi$  combinations cause collisions. They are the sterically forbidden values that bring atoms closer than their corresponding van der waal's distance.

The Ramachandran plot shows the sterically allowed values of  $\phi$  and  $\psi$  angles.

In the Ramachandran plot,

- Most areas are forbidden
- Only 3 small regions are physically accessible to most residues

## Still there are some exceptions

- ■Proline has cyclic side chain; rotation around C<sub>a</sub>—N bond is constrained by its inclusion in the pyrrolidine ring; values to angles around -60; Proline is the most conformationally restricted amino acid residue
- ■Glycine has no B carbon atom so least sterically hindered than other amino acids its permissible range covers a large area of the plot(even outside shaded regions)

  At glycine residues polypeptide chain often assumes conformations that are forbidden to other residues. So glycine frequently occurs in turn regions of proteins where any other residue would be sterically hindered.

8

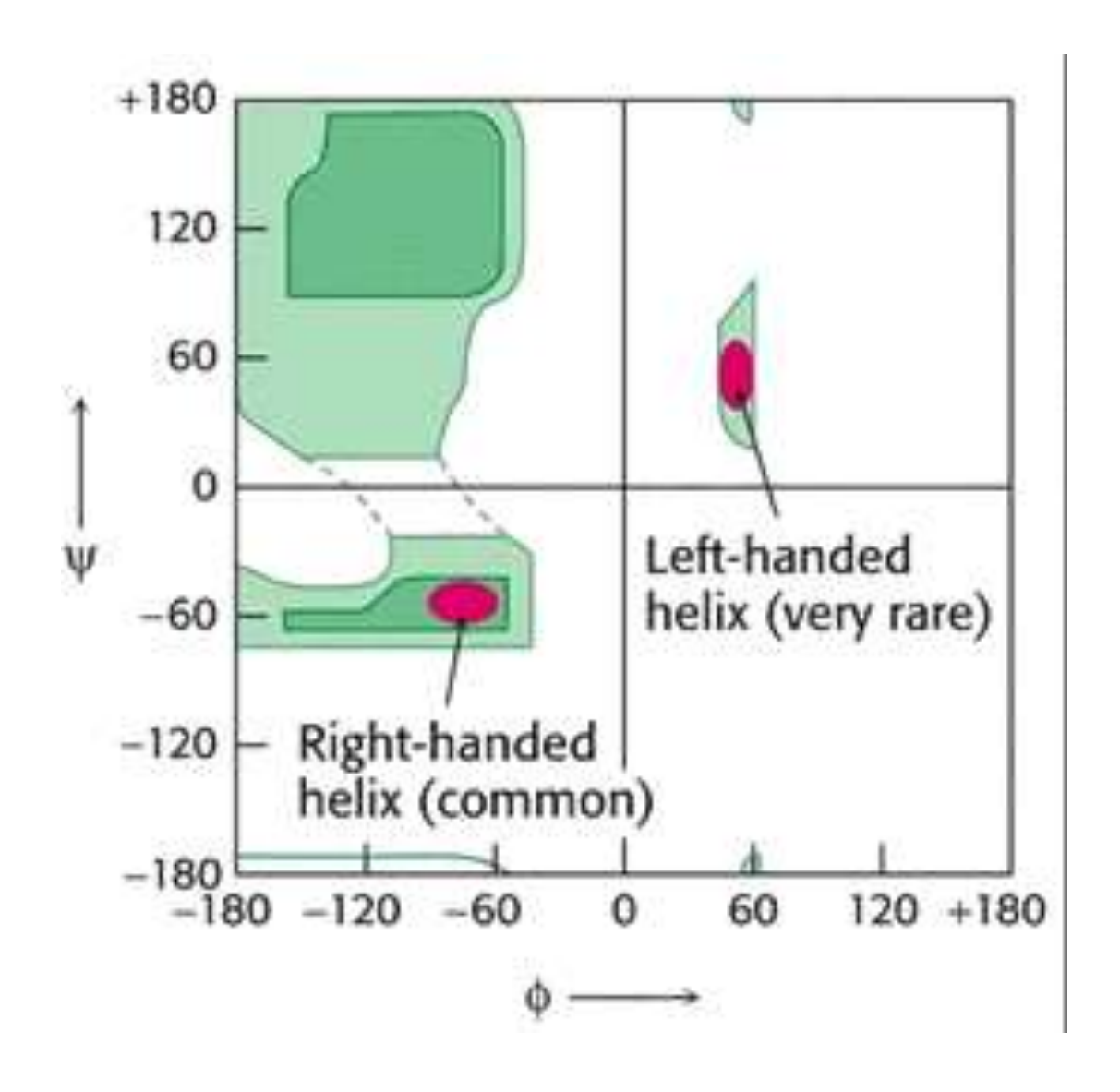
## Rama chandran plot for Alpha Helics and Beta Strands

## IN ALPHA HELIX,

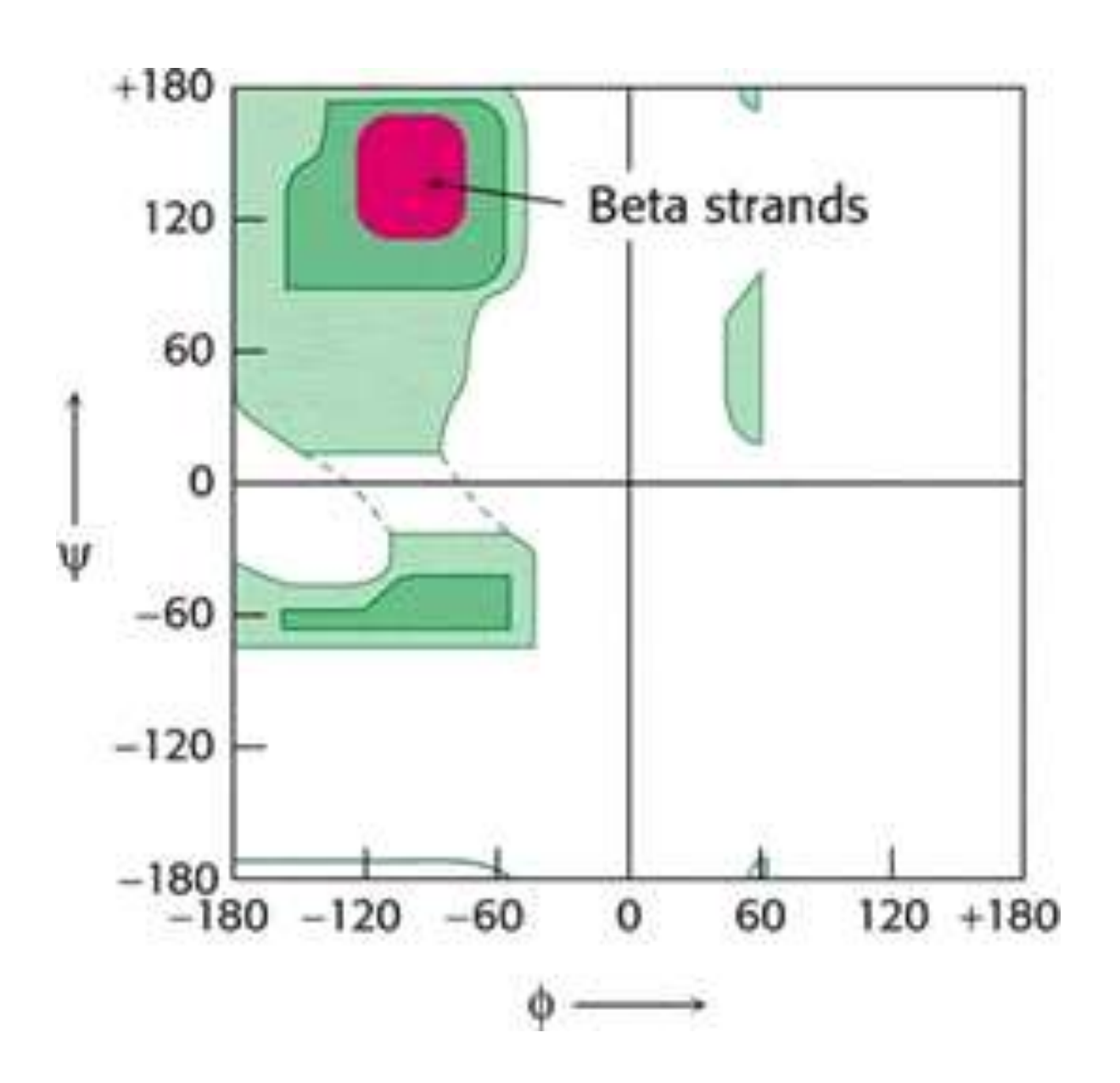
- The  $\psi$  and values of each residue are similar
- They cluster around a stable region of the Ramachandran plot , centered at a  $\phi$  of -57 to -60 and a  $\psi$  of -47 to -50 degrees
- This similarity gives alpha helix, a regular repeating structure.
- Also , the intramolecular H bonds between residues n and n+4 in alpha helices tend to 'lock in' rotation around the  $\phi$  and  $\phi$  bonds , restricting the  $\phi$  and  $C-C_{\alpha}$  angles to a relatively narrow range.
- ie., In alpha helix,

```
is \phi -40 to -100 degrees is \psi -40 to -65 degrees
```

## RAMACHANDRAN PLOT FOR ALPHA HELICES



## RAMACHANDRAN PLOT FOR BETA STRANDS



# Utility Of The Ramachandran Diagram

- R-diagram can be effectively used as a:
- Handy tool in data analysis on proteins such as motif recognition and closeness between two structures.
- Part of systematic study on hydrogen bonds in peptides segments.
- Check point during and after the crystal structure is solved.
- R-map concept can also be applied to other biopolymers such as nucleic acid and polysaccharides.

# Spectroscopy and its importance in chemistry

MSc –Semester II

(Course -CHE-CC-224)

## Dr. Pushpal Ghosh

**Assistant Professor** 

(Alexander von Humboldt Fellow)

School of Chemical Science and Technology,
Department of Chemistry
Dr. Harisingh Gour Vishwavidyalaya
(A Central University)
Sagar-470003, Madhya Pradesh

#### 1. Learning outcomes

After studying this module, you shall be able to:

- Why studying spectroscopy is necessary for chemist?
- Conceptualize electromagnetic radiation
- Understanding how energy is quantized
- To know the interaction of electromagnetic radiation and matters
- Outcome of various spectroscopy due to the different interaction

#### 2. Introduction

Many natural events create a tremendous curiosity since time immemorial. For example why rainbow appears in the sky, why colour of the sea or sky is blue? Why *aurora borealis* (*Northern Lights*) or *aurora australis* (*Southern Lights*) are seen only in the northern and southern region of the world unlike rainbow? Sir Isaac Newton in 1666 found that white light is separated into visible spectrum of primary colours when sunlight is passed through a triangular glass prism. The rainbow spectrum which are generated when sun's ray are scattered by raindrops may be called as the *electromagnetic spectrum*.

The interaction of electromagnetic radiation with matters (molecules/atoms) is one of the prominent technique called 'spectroscopy' to unravel many important properties specially atomic and molecular structures. Spectroscopy can give a good idea about molecular structure especially conformations, bond lengths, bond angles etc. For example, an analytical chemist can find the composition of a compound; an organic chemist use nuclear magnetic resonance spectroscopy in structural investigations whereas a physical chemist can use spectroscopy to detect reaction intermediates and to follow the concentrations of reacting species as a function of time. The 'luminescence' observed in fire flies or lighting materials of today's world like Compact fluorescence lamps, lasers, light emitting diodes (LED) are direct applications from the knowledge gathered from spectroscopy.

#### 3. Why we study spectroscopy?

Not much before, chemists used rigorous qualitative and quantitative experiments to understand chemical structure and compositions. These are time consuming, less precise and

normally use a large amount of samples (at least in the scale of gm). But spectroscopic techniques are rapid and less time consuming (sometimes in the range of seconds). They require very small amount of the samples and even they can be retrieved after experiment. Most importantly structural information obtained is much more precise, even very often their accuracy can be obtained in the micro or nanoscale level. Normally when an electromagnetic radiation especially 'light' hits a molecule/matter, following phenomenon occurs: molecule may absorb; scatter the light; some light may be transmitted through the molecules or some emission may come from the molecules. Now by measuring this absorption, scattering, transmission or emission chemist can understand the properties or structures of the molecule/matters.

#### 4. What is electromagnetic radiation?

Spectroscopy is conceived from the interaction of electromagnetic radiation and matter (molecule/matters). So it is pertinent to understand the electromagnetic radiation first. Thomas Young first observed interference of light in 1801when a beam of light was diffracted at two pinholes. His experiment proves the wave nature of light. Normally a wave requires a vibration in space and time. So obvious question is : what physical quantity is in vibrating in a light wave? Later in 1860s Maxwell relates the laws of electricity ad magnetism by a set of four differential equations which are famously called Maxwell's equation. These equation relates the electric (E) and magnetic (B) field vectors, the electric charge and the electric current. It is worthy to mention here that Maxwell's equations are the fundamental equation of electricity and magnetism as Newton's laws are fundamental equations of classical physics. Sometime later, in 1887, Maxwell's prediction of the existence of electromagnetic waves was confirmed by Hertz. He had generated electromagnetic waves in the metal wires of a tuned ac circuit by the oscillations of electrons and detected these waves by using a loop of wire. The oscillating electric field of the electromagnetic wave generates a time-varying force on the electrons in the wires of the detector circuit which eventually producing an alternating currents in these wires. It is evident from the Maxwell's equation that electromagnetic waves consist of oscillating electric and magnetic field. Let us consider electric and magnetic field vectors as E and B respectively which are perpendicular to each other and are perpendicular to the direction of travel of the wave (Figure 1). This figure depicts that an electromagnetic wave is travelling in the y direction. The wave shown in the figure can be depicted as plane polarized light because E vectors all lie in the same plane. This kind of plane polarized light can be produced by the back and forth oscillation of electrons in as straight wire. Here it must be mentioned that from the classical point of view, electromagnetic radiation is produced by an accelerated charge which is appropriate for the production of waves by electrons moving more or less freely in a metal wire. Normally such electrons have a continuous range of allowed energies. But the absorption and emission by atoms/molecules can generally be understood by using quantum mechanics. The quantum theory depicts a photon being produced or absorbed when an atom or molecule makes a transition between two allowed energy levels.

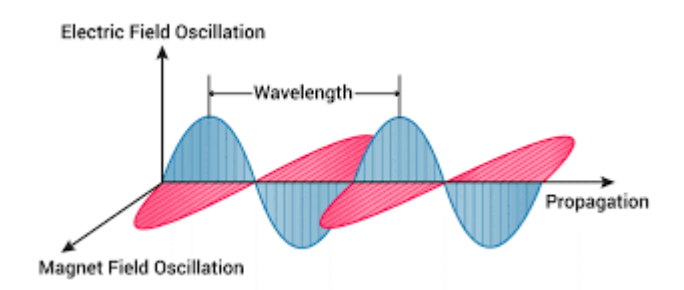


**Figure 1:** Electromagnetic waves consist of oscillating electric field and magnetic fields.

#### Source:

https://www.google.com/search?q=electromagnetic+radiation&source=lnms&tbm=isch&sa= X&ved=0ahUKEwjH7aXX\_vbgAhWGknAKHXOMBnkQ\_AUIDigB&biw=1366&bih=608 #imgrc=6mrWzosw5jpQrM:

#### 5. Quantization of energy

After successful experiment of Hertz and theory given by Maxwell a tremendous curiosity was developed by the end of 19<sup>th</sup> century to uncover the radiation theory. As 'ideal gas' theory is necessary to develop the theory of real gas, similarly Black body radiation was essential to understand radiation theory completely. A black body is an object which can absorb all the light when light is fall on a perfect black body. When the experimental result related to the energy density and wavelength are tallied with the theoretical result, it is observed that the result obtained from the theory based on classical physics do not match with the experimental results (Figure 2). Then several modifications were done by Stefan Boltzman, Wien etc. It was observed that Wein's law is valid for shorter wavelength but not for the longer wavelength. Then Raleigh-Jean's modification came. This postulates that an electromagnetic radiation consists of number of oscillators and each oscillator have energy KT *i.e.* energy is continuous. Though Raleigh-Jeans law is valid for higher wavelength but its fails for the shorter wavelength. In this context, Max Planck gave his revolutionary idea

that the energy of an oscillator is discontinuous and any change in energy content occurs only by means of a jump between two distinct energy states. This theory change the course of science from classical point of view and a new theory quantum mechanics came which covers range of areas from explaining atomic structure to spectroscopy. It can be easily said that 'spectroscopy' is a direct application of quantum mechanics.

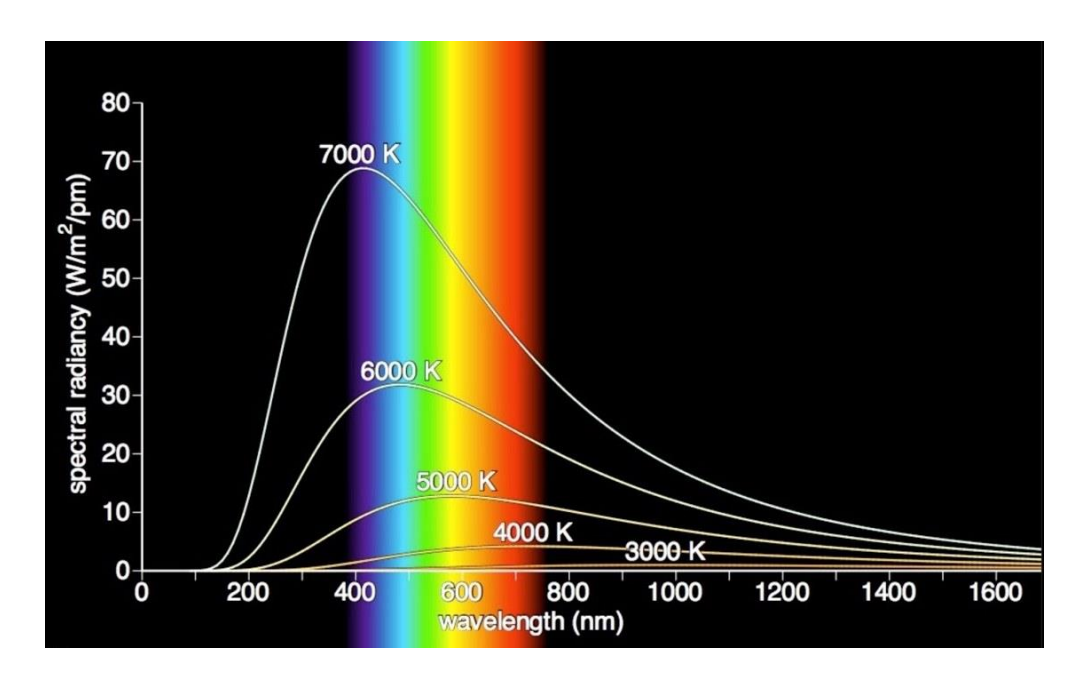


**Figure 2:** Relationship between spectral radiancy and wavelength obtained from black body radiation.

#### Source:

https://www.google.com/search?q=black+body+radiation&source=lnms&tbm=isch&sa=X&ved=0ahUKEwjw1tnDgPfgAhUQ3o8KHeNECEkQ\_AUIDigB&biw=1366&bih=608#imgrc=zMewqW1ZJwg3PM:

When a molecule rotate around it's centre of gravity, it may possess rotational energy. Similarly it may have vibrational energy due to periodic displacements of its atoms from their equilibrium position. In addition it may have electronic energy. As electron can exist in one or several discrete energy states, it can be said that energy is *quantized*. Likewise, rotational, vibrational and other sorts of energy of a molecule are also quantized and a molecule can move from one level to another level by a sudden jump with taking certain amount of energy.

Normally in spectroscopy we study the absorption and emission of light (electromagnetic radiation) with matters. The range of frequencies abosorbed by a molecule is its *absorption* 

spectrum; the frequencies emitted constitute *emission spectrum*. Normally a *line spectrum* consists only discrete frequencies. However a *continuous spectrum* contains a continuous range of frequencies. Quantum mechanical treatment depicts that when a sample is exposed to electromagnetic radiation; it may absorb a photon of frequency  $\gamma$  and can move to a higher energy state. If the ground state is designated as 'a' and upper state as 'b', it can be easily said that  $E_a$ - $E_b$ =  $h\gamma$ . Similarly a molecule in upper state 'b' can spontaneously move to state 'a' by emitting a photon whose energy satisfies  $E_b$ - $E_a$ = $h\gamma$ . This is called spontaneous emission of a radiation (**Figure 3**).

So we can write  $\gamma = \Delta E/h$  Hz

Or  $\Delta E = h\gamma$  joules (where h is a Planck's constant and its value is 6.63X  $10^{-34}$  joules s molecule<sup>-1</sup>).

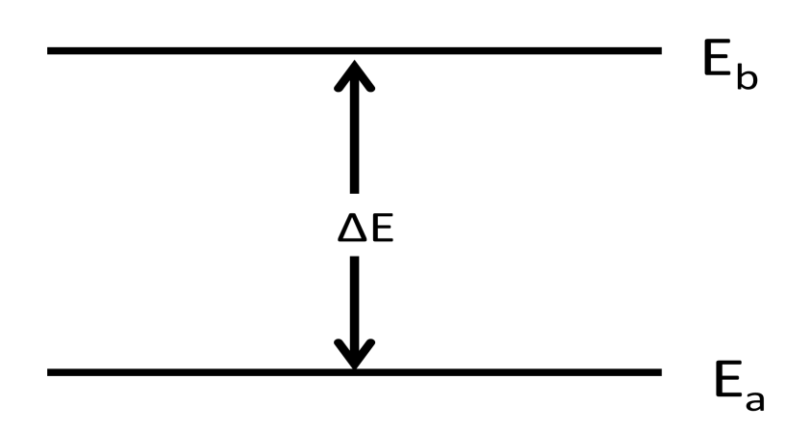
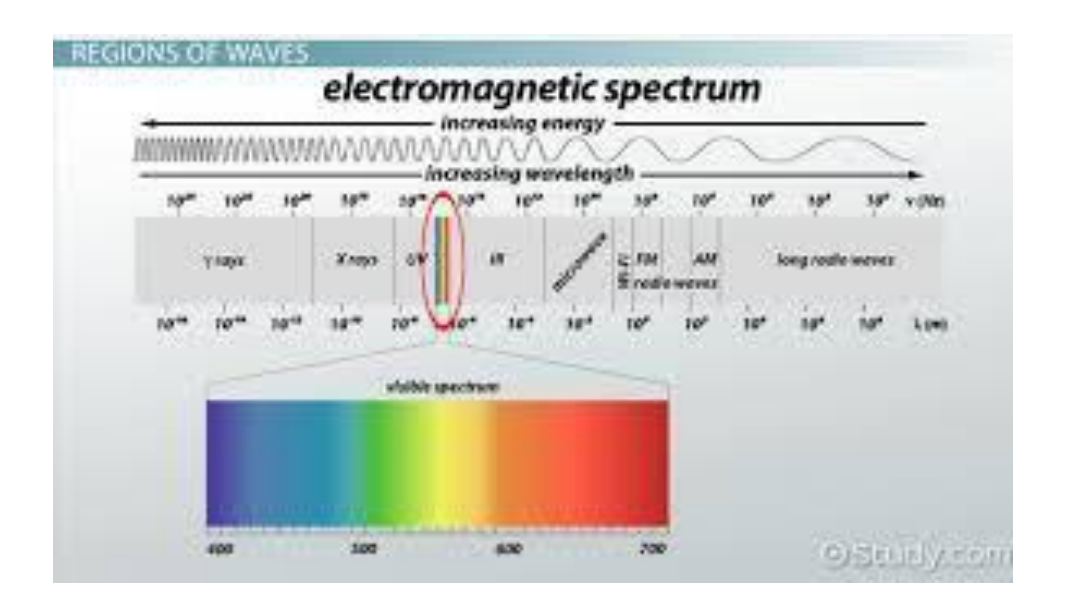


Figure 3: Transition between two energy levels.

#### 6. Regions of electromagnetic spectrum and associated spectroscopy

Figure 4 shows the schematic diagram showing various regions into which electromagnetic radiation is divided. Though the boundaries between different regions are arbitrary but the molecular processes associated with each region are specific and different. Hereby it is depicted each region in increasing frequency or energy.



**Figure 4:** The regions of the electromagnetic spectrum

#### Source:

https://www.google.com/search?q=different+regions+of+electromagnetic+radiation&source=lnms&tbm=isch&sa=X&ved=0ahUKEwingsKY0PbgAhWOWX0KHc20DXwQ\_AUIDigB&biw=1366&bih=657#imgrc=ColuVdu04h5cdM:

- 1. Radiofrequency region and occurrence of Nuclear magnetic resonance/electron spin resonance spectroscopy
  - The radiowaves have lowest frequencies or lower energies (highest wavelengths). Energy ranges from 10 m-1cm and energy changes involved is coming out from reversal of spin of a nucleus or electron. Here it may be considered that the nucleus and electron are tiny charged particles and their spin can be associated with a magnetic dipole. Now the reversal of this dipole followed by spin reversal and interaction with the magnetic field of the electromagnetic radiation at appropriate frequency can result NMR or ESR spectroscopy.
- 2. Microwave region and Rotational spectroscopy: Energy ranges in Microwave regions are between 1cm-100 μm. The molecules which have a permanent dipole moment like HCl is microwave active and can show rotational spectra. When HCl molecule is rotated, it can be seen that plus and ninus charges change places periodically and the component of dipole moment fluctuates regularly. Now when interaction occurs, energy can be absorbed or emitted in the form of rotational spectrum. The best example in day to day life is the use of microwave oven in our kitchen. Normally in conventional cooking, first

- peripheral part of the food materials is heated and then inside is cooked. But cooking using MW oven is different. Here water molecules which have permanent dipole moment are normally stay in plenty amount in food material and can rotate contrary to the large size biological molecules. Now the excess rotational energy of the water molecules is reemitted as heat and the food materials are cooked from inside.
- 3. Infra-red region and vibrational spectroscopy: Energy ranges in Infrared regions are between 100 μm-1μm. This is one of the most important spectroscopic regions for chemist specially for understanding the presence of different functional groups by FTIR spectroscopy. Instead of rotation, here it is a vibration which must cause a dipole change in the molecule to be infrared active. For example 'symmetric stretch' mode of vibration for CO<sub>2</sub> molecule is 'infra red in active', however both the 'bending' and 'asymmetric' mode are 'infra red' active.
- 4. Visible and Ultraviolet region: Normally ranges between 1000 nm-800 nm are considered as Near Infra Red (NIR) region. However ranges from 800 nm-400 nm is called Visible region and from 400-10 nm is within Ultraviolet region. Electronic spectroscopy arises in these regions. Normally excitation of a valence electron causes the moving of electronic charges in the molecule. Then the subsequent change in the electric dipole causes rise of a spectrum by the interaction with the undulatory electric field of radiation.
- 5. X-ray region: This region comes in one of the high energy region and it ranges from 10 nm-100pm wavelength. Energy changes in this region normally involve inner electrons of an atom or a molecule. Normally X-ray beam is produced by electron bombardment of a clean metal target like Al, Cu, Mg, Fe etc., resulting in the emission of radiation at very specific energies. For example,  $k_{\alpha}$  line for Al occurs at 1486.6 eV
- 6. γ-ray region: After X-rays, this region in very high energy comes and the range of this region is in between 100pm-1pm. Here energy changes involve the rearrangement of nuclear particles. Mössbauer spectroscopy which was named after its discoverer who won a Nobel prize in 1961 is involved in this region.
- 7. Raman spectroscopy: Raman spectroscopy discovered by Sir C.V. Raman who won the Nobel prize yields information similar to the obtained in the microwave and infra-red regions. However experimental method is such that the observations can be made in the visible region. The only condition for the molecule to be Raman active is that the molecule must have polarizability.

#### 7. Summary:

In this module we have learnt:

- Several natural phenomenon like occurrence of Rainbow, aurora borialis, colour of the sky and sea, chemiluminescence of fire flies etc. come in the ambit of spectroscopy.
- Compared to other techniques for the detection and analysis of chemical compounds, spectroscopic techniques are fast, non-destructive and use lesser amount of chemicals.
- Molecular spectroscopy arises due to interaction of electromagnetic radiation and molecules/matter.
- Electromagnetic waves consist of oscillating electric and magnetic field. The
  oscillating electric field of the electromagnetic wave generates a time-varying force
  on the electrons in the wires of the detector circuit which eventually producing an
  alternating currents in these wires.
- It is understood how the experimental observation from black body radiation is not satisfied by the concept of classical mechanics. It was observed that Wein's law is valid for shorter wavelength but not for the longer wavelength. However, Rayleigh-Jeans law is valid for longer wavelength but not for shorter wavelength.
- In this context, Max Planck gave his revolutionary idea that the energy of an oscillator is discontinuous and any change in energy content occurs only by means of a jump between two distinct energy states.
- Quantum mechanical treatment depicts that when a sample is exposed to electromagnetic radiation; it may absorb a photon of frequency  $\gamma$  and can move to a higher energy state. Similarly a molecule in upper state can spontaneously move to lower state by emitting a photon.
- Now different region of spectrum and its concerned spectroscopy is discussed.

The arrangement of different regions of electromagnetic radiation with increasing order of their wavelength is: γ-rays<X-rays<UV rays<Visible light<Infrared rays<Microwave rays<Radio waves.

# Wave particle duality

MSc –Semester II (Course –CHE-CC-224)

# Dr. Pushpal Ghosh

**Assistant Professor** 

(Alexander von Humboldt Fellow)

School of Chemical Science and Technology,
Department of Chemistry
Dr. Harisingh Gour Vishwavidyalaya
(A Central University)
Sagar-470003, Madhya Pradesh

### TABLE OF CONTENTS

- 1. Learning outcomes
- 2. Introduction
- 3. Photoelectric effect
- 4. de- Broglie hypothesis
- 5. Heisenberg uncertainty principle
- 6. Summary

### 1. Learning outcomes

After studying this module, you shall be able to understand:

- How the concept of wave-particle duality arises in the quantum mechanics?
- Conceptualize photoelectric effect
- Understanding de Broglie's hypothesis and its significance
- Heisenberg's uncertainty principle

#### 2. Introduction

Wave-particle duality is a very important concept which states that every particle or quantum entity can be described in terms of not only waves but also as particles. But the development of this important concept took long time specially centuries. Ibn al-Haytham, an Arabic Scientist in 11<sup>th</sup> Century demonstrated in his book named 'Book of Optics' that the light or rays were composed of particles of light. Sir Isaac Newton developed corpuscular theory of light and emphasized that the perfectly straight lines of reflection indicates particle nature of light. Around the same time, Huygens, Robert Hook and later Fresnel developed the wave view point mathematically and their views were supported by Thomas Young's discovery of wave interference of light by his famous double-slit experiment in 1801. In 1860s James Clerk Maxwell applied his equations to describe self-propagating waves of oscillating electric and magnetic field and very soon it was perceived that visible light, ultraviolet light and infrared light are all electromagnetic waves with different frequency. Again in 1887, Maxwell's prediction of the existence of electromagnetic waves was confirmed by Hertz which was explained in my last lecture. So it was not clear to the scientific community until first end of twentieth century about actual nature of light.

#### 3. Conceptualize photoelectric effect

Earlier black body radiation and quantization of energy is nicely explained by Max Planck. While Max Plank had solved the ultraviolet catastrophe by using a quantized electromagnetic field, but there were some issues still. However, Einstein used Plank's black body model to solve another important problem of that time called photoelectric effect wherein electrons are emitted from atoms when they absorb energy from light and would lead to an electric current in a circuit. Albert Einstein 1905 gave an explanation of the photoelectric effect which was not explained by the wave theory of light. Einstein postulated the existence of photons and quanta of light energy with particulate qualities. First it was assumed that light was knocking the electrons. But in case of potassium, it was observed that a dim blue light was able to create current however brightest red light was not able to create that current. This observation was certainly not according to the classical theory which says that strength of amplitude of a light wave is in proportion to its brightness i.e. a bright light should easily create a large current. But this was not observed in case of potassium when bright red light was used.

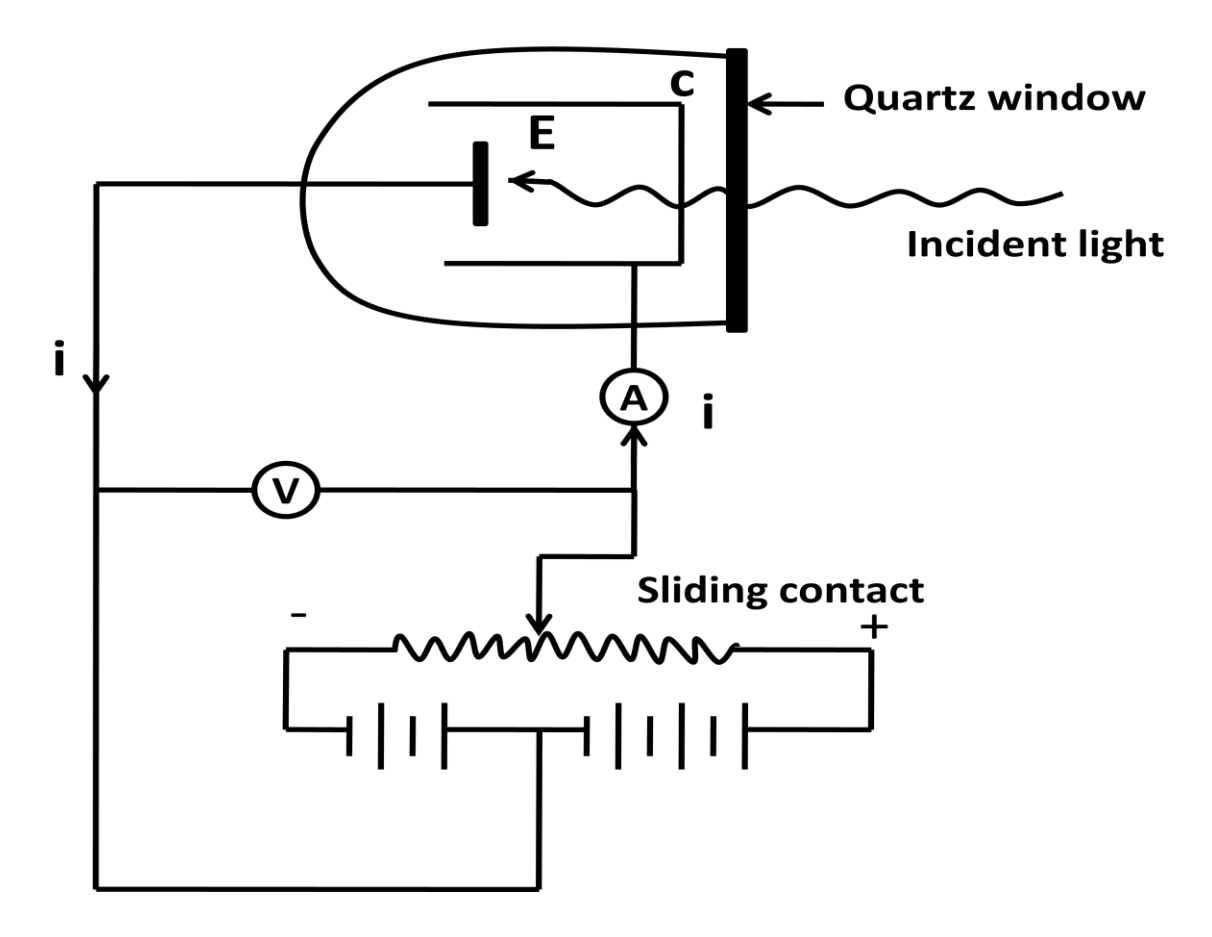


**Figure 1.** A schematic diagram showing photoelectric effect.

#### Now let us discuss the photoelectric effect.

Light of frequency  $\upsilon$  hits the emitter E and with the help of a potential difference V between the E and the collector C, photoelectrons and photoelectric current can be produced and measured (Figure 1). Figure 2 depicts a plot of i vs V. It is seen that with increase of V, i increases and finally reaches a constant saturated value (curve a). Now if V is made zero, i does not come down to zero. This happens because electrons are emitted with certain velocity and may reach the collector on their own urge. But i can be made zero by reducing the potential to a negative value  $V_o$  which is called as Stopping potential. Now this  $V_o$  times the charge of an electron gives the kinetic energy of the most energetic photoelectrons.

$$K_{max} = eVo$$

Now keeping  $\upsilon$  unchanged, if the intensity of the light is doubled though the saturation current gets doubled but  $V_o$  remains the same. So it can be said that  $V_o$  and  $K_{max}$  are both independent of light.

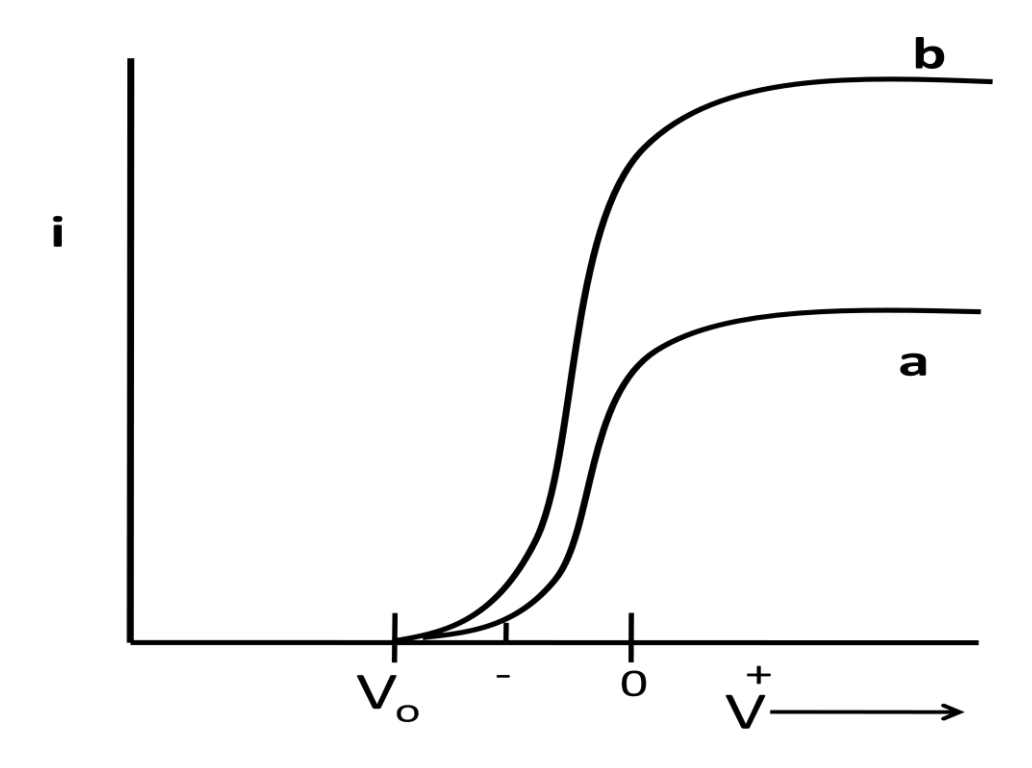


Figure 2: Variation of current vs stopping potential.

Now Figure 3 shows the variation of the stopping potential vs  $\upsilon$ . A straight line is obtained and there is a threshold cut off frequency at which  $V_o=0$  is observed. No light below this frequency, however high intensity it has, is able to produce photoelectrons.

Three special features related to photoelectric effect which cannot be explained in terms of classical physics are given below.

- 1. The intensity problem: From the classical point of view, as the intensity of the light is increased, the amplitude of the oscillating electric field also increases. Since the force exerted on the electron is eE, this suggests that the kinetic energy (KE) of the photoelectrons must also increase with the intensity of light. But it is found from the experiment that  $V_o$  and  $K_{max}$  is independent of the intensity of the light.
- 2. **The frequency problem:** Classical physics expects that photoelectron can be ejected for any frequency of light, provided it is intense enough to expel the electrons from under the skin of the metal. But experiment which is mentioned above shows that for each surface there is a cut off frequency below which the photoelectric effect does not occur, no matter how the intense the illumination.

3. **The time lag problem:** A definite time lag is required for an electron to soak up sufficient energy from the wave front. But the above experiment suggests that there is no time lag between the incidence of light and ejection of the photoelectrons. Both the process is instantaneous.

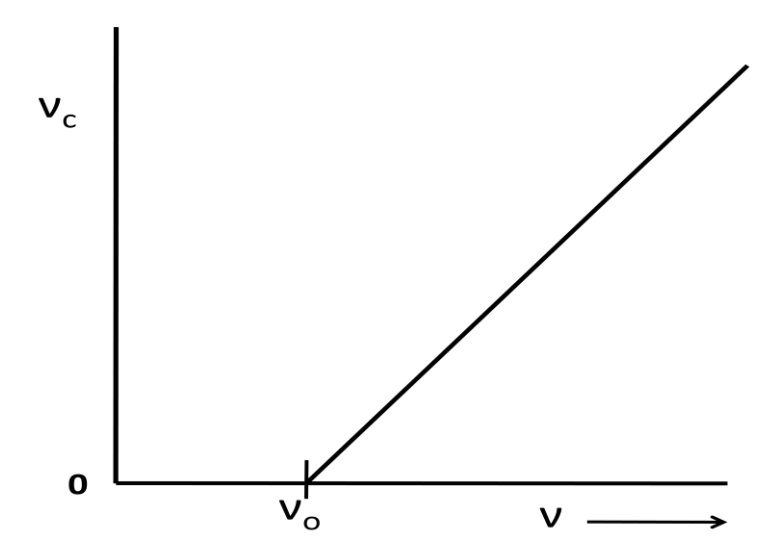


**Figure 3:** Variation of stopping potential vs υ.

Now Albert Einstein solved these issues with his new approach. He pointed out that radiation is itself quantized. The light beam consists of packets of energy known as photons. The energy of a single photon is  $h\nu$ , where  $\nu$  is its frequency. So by increasing intensity of a light beam means an increase in the no of photons per unit volume.

Now in order for an electron to be ejected, it must receive energy equal to its binding energy, the work function for the metal involved. If the frequency is so low that ho is less than the work function, then electron can't be ejected, hence the threshold frequency is important.

The work function  $\Phi = h\nu_0$ , here h is Planck's constant  $(6.626 \times 10^{-34} \text{Js})$ 

Emission occurs only when  $h\nu$ > $\Phi$ , and any excess of  $h\nu$  over  $\Phi$  appears as the KE of the electron.

So we can write  $K_{max} = h\upsilon - \Phi$ 

$$V_o = hv/e - \Phi/e$$

 $= hv/e - hv_0/e$ 

This was actually observed in figure 3.

Finally since the photons are concentrated energy bundles and the transfer of energy from the radiation has been through a photon transferred to its entirely to a single electron, no time lag is observed between the incidence of light and the ejection of electron. In 1921, Albert Einstein was awarded Nobel prize in Physics for his discovery of the law of the photoelectric effect.

#### 4. Understanding de Broglie's hypothesis and its significance

Researchers are always been fascinated by the symmetry of the world. Light which was considered to be a wave is now have a particle like behaviour as explained in photoelectric effect. So it is not unwise to expect particles having wave like properties. In 1924, Louis de-Broglie, proposed that just as light has both wave-like and particle-like properties, electrons also have wave like properties. So it can be hypothesized that with any moving body there is associated a wave and that the momentum of the particle and the wavelength of the associated wave are related by

$$\lambda = \frac{h}{p}$$

Now this can be proved by the following way.

Energy 
$$E = \sqrt{m^2c^4 + p^2c^2}$$

Where m = rest mass and p is the monetum

For a photon E = hv and m = 0

So hv = pc

$$\frac{c}{v} = \lambda = \frac{h}{p}$$

This dual character of the matter i.e. matter wave were first experimentally demonstrated by George Paget Thomson's cathode ray diffraction experiment and the Davisson-Germer experiments for electrons. In 1927, at University of Aberdeen, G.P. Thompson observed the diffraction of electrons by a thin film of celluloid. Eventually his father J.J. Thompson was awarded the Nobel prize for showing that electrons are particles and he himself along with

Davisson shared the Nobel prize for Physics in 1937 for their experimental work. De-Broglie was also awarded Nobel prize for Physics in 1929 and his formula was confirmed three years later in a brilliant experiment designed by Clinton Joseph Davisson and Lester Halbert Germer at Bell Laboratory. They fired slow moving electrons through a double slit at a crystalline nickel target and then measured the angular dependence of the diffracted electron intensity. The same diffraction pattern as those predicted by Bragg for X-rays was observed. So both these experiments proves de-Broglie's hypothesis of dual character of matter both as a particle and matter.

#### Electron as a matter wave and Bohr's momentum qunatization:

Now let us consider a electron in an orbit. Then for most momenta and radii, the waves associated with the particle will interfere destructively as they overlap round each orbit; only for some radii and momenta will the ends of the waves on each orbital circuit join, so that non destructive interference occurs. For this to occur, the circumference of the orbit must fit an integral no of the wavelength of the wave associated with the electron.

Then the condition will be

$$2\pi r = n\lambda$$
 where n = 1, 2, 3.....

Using this in the de-Broglie equation,

$$\lambda = \frac{h}{p}$$

$$\lambda = \frac{h}{mv}$$

$$\frac{2\pi r}{h} = \frac{h}{mv}$$

or 
$$mvr = \frac{nh}{2\pi}$$

This is called the momentum quantization of Bohr.

#### 5. Heisenberg uncertainty principle

A significant problem in classical mechanics is the finding of the values of various dynamical variables of a system like momenta and co-ordinates, energy and time at one instant. Generally the motion of a system of f degrees of freedom requires the knowledge

of f-momenta and f-position coordinates. It is also normally considered in classical mechanics that this entire 2f variable can be determined with any desired degree of accuracy. Actually this is not true.

In this context, Werner Heisenberg postulated his uncertainty principle. The principle says that for each system there are certain sets (member = 2) of conjugate variables, like x position coordinate and x component of the linear momentum, energy and the time coordinate, angular momentum along two axes, say x and y, which cannot be determined simultaneously, there will always be certain uncertainties in their values so that, the product of the two uncertainties will be either greater or at least equal to  $\hbar/2$ .

$$\Delta x.\Delta p_x \ge \hbar/2$$

$$\Delta y.\Delta p_y \ge \hbar/2$$

$$\Delta E.\Delta t \geq \hbar/2$$

$$\Delta M_x \cdot \Delta M_y \ge \hbar/2$$

 $\Delta$  here indicates standard deviation, a measure of spread or uncertainty.

Heisenberg eventually explained this phenomenon as a consequence of the process of measuring i.e. measuring position accurately would disturb momentum and vice versa. This was diligently confirmed by the so called "gamma-ray" experiment which crucially depends on de Broglie hypothesis. So the idea of uncertainty principle directly comes out from the wave-particle duality.

#### **Summary**

In this module we have learnt:

- Several important observations where every particle or quantum entity can be described in terms of not only waves but also as particles.
- Black body radiation, quantization of energy and specially ultraviolet catastrophe can be nicely explained by Max Planck's theory.
- It is explained in the lecture how Einstein used Plank's black body model to solve another important problem of that time called photoelectric effect wherein

- electrons are emitted from atoms when they absorb energy from light and would lead to an electric current in a circuit.
- Einstein has shown that not only the intensity of light however the frequency of the light is important for releasing the photoelectrons.
- Einstein theory nicely solved the intensity, frequency and time lag problem which can not be solved by the classical outlook.
- Louis de-Broglie's hypotheis proves that just as light has both wave-like and particle-like properties, electrons also have wave like properties. This was further proved experimentally by Davission and Germar and G. P Thompson separately.
- Bohr's momentum quantization is nicely explained using de-Broglie's hypothesis.
- Now finally Heisenberg's uncertainty principle is discussed. The principle says that for each system there are certain sets (member = 2) of conjugate variables which cannot be determined simultaneously. There will always be certain uncertainties in their values so that, the product of the two uncertainties will be either greater or at least equal to  $\hbar/2$ .

# Characterization techniques for nanomaterials

MSc –Semester IV

(Course -CHE-CC-428)

### Dr. Pushpal Ghosh

**Assistant Professor** 

(Alexander von Humboldt Fellow)

School of Chemical Science and Technology,
Department of Chemistry
Dr. Harisingh Gour Vishwavidyalaya
(A Central University)
Sagar-470003, Madhya Pradesh

In this module, different synthesis protocols used for preparing the nanocrystals via templating agents like ionic liquids etc. are illustrated. It is well known that ionic liquids not only play a pivotal role as capping or templating agent in controlling the nucleation and growth of nanocrystals, but these are also used as solvent and reaction partner during the synthesis. Synthesis of nanoparticles and tuning of shape, size and optical properties of semiconducting (band gap) and rare-earth doped nanocrystals using the ILs are also illustrated in details. This chapter comprises parts in which first introduction about the ionic liquids (ILs) and then hydrothermal/solvothermal methods are explained.

#### 2.1 Ionic liquid

Few years before, organic solvent and long chain containing organic surfactants were substantially used for synthesis and designing of nanoparticles with desired properties like phase, shape, size and optical properties. The foremost issues with these organic compounds or solvents are less stability (both thermally and chemically), very high vapour pressure, highly flammability and causing severe hazardous affect on the environment and human being. Owing to overcome all these limitations, ILs have been used as an alternative of organic solvents and surfactants. ILs are the combination of cation and anion and exist in liquid state in ambient conditions (at room temperature and in normal atmospheric pressure, Figure 1).<sup>2-6</sup>

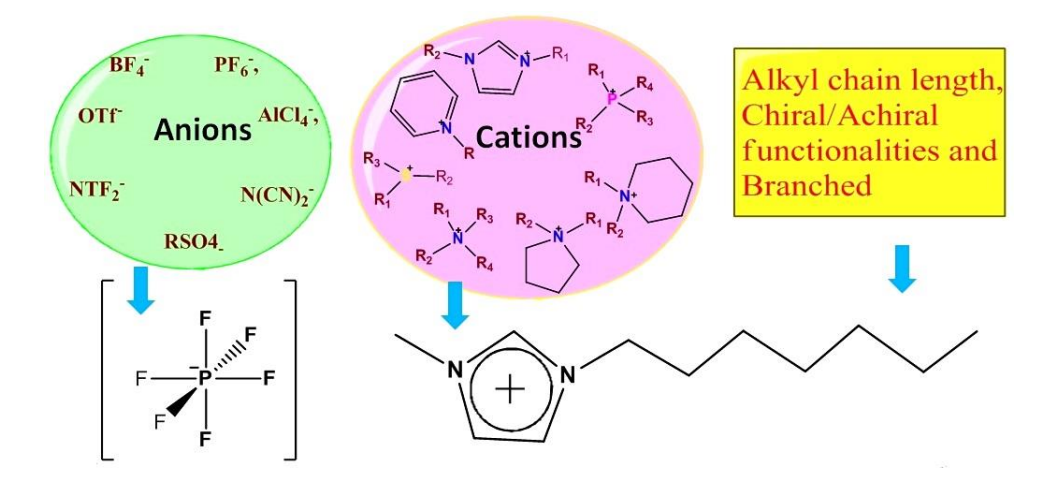


**Figure 1.** Schematic representation of tuning the ionic liquid using cation-anion combination, and alkyl chain length.

Past of the ILs could be dated back to a century ago, when triethylammounium nitrate was considered as first ionic liquid, pure low-melting salt.<sup>2-4,7</sup> 1n 1930s, molten pyridinium salt

was used for cellulose dissolution above 130°C.<sup>7</sup> Owing to lower down their melting point and other physical and chemical properties, cation and anion combination was tuned. Especially imidazolium based cation would be used for tuning the cation nature because it has N-atom in aromatic ring system which can be attached to different alkyl chain. On another side, bis(trifluoromethylsulponyl) amide (CF<sub>3</sub>SO<sub>2</sub>-N-SO<sub>2</sub>CF<sub>3</sub>, also known as NTf<sub>2</sub>) ions was used with combination of ethylmethylimidazolium cation to lower down the melting point till -15°C.<sup>7,8</sup> Symmetry of cation and flexibility of anions have pivotal impact on the physical and chemical properties of ionic liquid.<sup>7</sup> In addition, there are other numerous factors for instances bulky cation and charge-delocalized anions, thermodynamically high solvation free energy and high entropy, which do not allow them to be crystallized in ambient condition.<sup>7,9</sup> In this way, most of the ILs are liquid. Ionic liquids have numerous physical

properties such as large liquidus range, wide electrochemical window (in some cases it can be spanned 6V) up to flammability, thermally stable and pressure.<sup>7</sup> negligible vapour

Zwitterionic Aprotic Ionic-liquid-based Lithium batteries Fuel cell membranes and supercapacitors

**Ionic Liquids for Specific Applications** 

Protic

These properties can be tuned by judicious selection of cation-

**Figure 2.** Figure represents the specific applications of different ionic liquids (ILs)

anion combination, changing the alkyl chain length and concentration of IL.<sup>7</sup> On the basis of judicious combination of cation and anions, several ionic liquids can be designed for specific applications such as aprotic types of liquid which is basically used for lithium ion batteries and supercapacitors. However protic IL is suitable for fuel cell and zwitterionic types of ILs are employed for IL-based membranes (Figure 2). As a result, ILs are considered as potential candidate for numerous applications like energy application, catalysis, lubricant, solar cell, batteries, surfactant, reaction partner and nanomaterial synthesis. 7,10-14

In 1992, Wilkes and Zaworotko discovered the water soluble ionic liquid, afterward it was widely applied for catalyzing the organic synthesis and organometallic reactions. <sup>15</sup> In beginning, it was used as a reaction medium in place of conventional organic solvent for performing the syntheses. Dai et. al pioneered the application of ionic liquid in synthesis of inorganic based materials. 16 Dupont's group have prepared uniform Ir nanoparticles using [Bmim] PF<sub>6</sub> ionic liquid as a reaction media. In 2004, Morris and Taubert proposed "ionothermal" and "all-in-one" concept for preparation of inorganic materials using IL as a

solvent. <sup>18,19</sup> On the basis of different mode of interactions between ILs and material, there are many advantages of using ILs as a solvent over the conventional solvents and that have been realized for the preparation of inorganic materials. For instances: (i) IL induces high nucleation rate due to low interface tension, (ii) they affect the structures of resultant materials via forming the extended hydrogen bond in solution phase; and (iii) owing to have tunable property, high polarity and insolubility in organic solvent, it can be alternative of two phase system. <sup>14</sup>

In inorganic based nanomaterial synthesis, ionic liquids play a very crucial role in designing of nanoparticles with desired properties, where it can be used as reaction medium, reaction partner and capping or templating agent. Alkyl chain length and nature of anion of IL have significant effect on controlling dispersity, particles size and morphology of metallic nanoparticles. 19-26 Ionic liquid (as a solvent) not only stabilizing the metallic nanoparticles but also assist in reducing metal ion to form metallic cluster. Interestingly, ionic liquid [Bmim]+PF<sub>6</sub> is also utilized for dispersion of graphene sheet which was stabilized by polymerized IL.<sup>27</sup> On the other hand, several semiconducting nanoparticles have also been synthesized using the ILs, in which IL is used as reaction medium and stabilizers to inhibit the aggregation of nanoparticles. In addition, it is also used as a capping and templating agent to govern the size, phase and morphology of nanoparticles which can be attributed to interaction of IL with nanoparticles via aromatic π- system, hydrogen bonding through acidic hydrogen and interaction of anions.<sup>13</sup> Furthermore, by judicious selection of counter ion (anions) of ILs, it can also be employed as reaction partner for the synthesis of various types of nanomaterials. These anions could be BF<sub>4</sub>, PF<sub>6</sub> for the source of fluoride (F) ion, [H<sub>2</sub>PO<sub>4</sub>]<sup>-</sup> for phosphate ion (PO<sub>4</sub><sup>3-</sup>), and [SeO<sub>2</sub>(OCH<sub>3</sub>)]<sup>-</sup> as source of selenide (Se<sup>2-</sup>) ion for fabricating the fluoride, phosphate and selenide based nanoparticles respectively. 14,28-35 For instances, BF<sub>4</sub>, PF<sub>6</sub> ions consisting ionic liquids have been significantly employed for the synthesis of fluoride based nanoparticles (especially binary and ternary rare-earth doped fluoride nanoparticles). 28-29 Phosphate-based nanoparticles such as Eu doped YPO<sub>4</sub>, LaPO<sub>4</sub> and GdPO<sub>4</sub> were prepared using the [cholin][H<sub>2</sub>PO<sub>4</sub>] ionic liquid.<sup>33</sup> In addition, BiOBr and BiOI nanoparticles have been prepared using the [C<sub>16</sub>mim]Br and [Bmim]I ILs respectively as precursor of Br and I ions. 34-35 On the other hand for synthesis of selenium based nanoparticles such as ZnSe, CdSe and Cu<sub>2</sub>Se having different morphologies were designed by using [Bmim]<sup>+</sup> [SeO<sub>2</sub>(OCH<sub>3</sub>)]<sup>-</sup> as a Se precursor.<sup>30-31</sup> In this way, ILs have drawn a tremendous importance in the field of nanomaterial engineering.

#### 2.1.1 Ionic liquid (IL) assisted hydrothermal/solvothermal synthesis

Now-a-days, hydrothermal/solvothermal method is a frequently used method for the synthesis of materials with desired properties such as crystal phase, size, morphology and so on. When water is heated above its boiling point in a compactly closed vessel, it exerts tremendous amount of pressure in reaction container. At such high temperature and pressure inside the vessel, IL plays a vital role in the conversion of reactant into the required product. Thus hydrothermal process can be illustrated as heterogeneous reaction which is taken place in aqueous medium above the boiling point of water (above 100°C and 1bar). Before, this reaction process was used by geologist and mineralogist to study the formation of minerals in nature. However, in industries this reaction process was used as hydrometallurgy, in other way, it is also known as classic Bayer process for the decomposition of bauxite. In order to tune the property of the material especially at nanoscale, controlling of nucleation rate is pivotal which is substantially governed by the reaction temperature, time, medium, surfactant and pressure. Instead of water, other solvent is used as a reaction medium, and then it is called solvothermal method. The surface of the decomposition of medium, and then it is called solvothermal method.

Task specific ionic liquid (TSIL) mediated solvothermal/hydrothermal synthesis method are being rapidly used for the preparation of wide range of nanomaterials for instances, metal chalcogenides such as CdS, 3D flower like CuS microflowers, bismuth oxyiodine (BiOI) microspheres, NiFe<sub>2</sub>O<sub>4</sub> nanorod–graphene composite, hybrid nanomaterials like 3D CuS ordered nanoerythrocytes/rGO composite, upconverting Yb and Er doped YF<sub>3</sub> etc.<sup>38-43</sup>

Hydrothermal/Solvothermal reaction chamber (autoclave)



**Figure3.** Autoclaves hydrothermal synthesis slab.

In order to perform the hydrothermal/ solvothermal reaction, special type of reaction chamber is used which is known as autoclave, and is used for the synthesis of inorganic nanocrystals at elevated temperature and high pressure. In 1879, Charles

Chamberland invented this device.<sup>44</sup> Previously, it was used for sterilizing equipment and in chemical

industry to cure coating, vulcanize rubber. Generally, for nanomaterial synthesis, the design of autoclave is very important especially related to the chemical inertness. Therefore, this reaction chamber mainly consists of outer cylindrical jacket which is made up of thick-walled

steel owing to withstand at high temperature and pressure for prolong time and inner inert cylindrical Teflon chamber to put the reaction mixture. Figure 3 shows image of autoclave used during the nanomaterials synthesis via hydrothermal/solvothermal process.

#### 2.2 Characterization techniques

After preparing nanomaterials, it is very important to elucidate their structure, and their properties. By Powder X-ray diffraction study, we can identify the crystal phase of the nanomaterials, can measure the volume fraction, crystallite size, lattice parameters etc. Microstructural study can be obtained from Transmission Electron Microscope images (TEM). High Resolution Transmission Electron Microscope (HRTEM) images can predict the growth mechanism of the nanocrystals from the atomistic origin. Morphology of the nanostructures can be determined from scanning electron microscopy (SEM and FESEM). From FTIR study, structural information can be obtained. BET surface area analyzer can be used to estimate the surface area of the nanocrystals. Optical absorption spectroscopy and photoluminescence (PL) were used to understand the electronic transitions in the rare-earth doped nanoparticles. Time correlated single photon counting (TCSPC) was used to understand the relaxation dynamics of the rare-earth ion.

This section is used to explain the basic principles and techniques used for the characterization of the nanomaterials.

#### 2.2.1. Powder X-ray diffraction method (PXRD)

In Powder X-ray diffraction, electromagnetic wave in the region of X-rays is used. Here wavelength is usually measured in angstrom ( $1A^{\circ} = 10^{-10} \,\mathrm{m}$  or  $10x10^{-9} \,\mathrm{m}$ ) and its photon energy is in the range of  $100\mathrm{eV}$ - $100\mathrm{keV}$ . This wavelength range is in the size of atom. After discovery of X-ray by William Rontgen in 1895, it facilitated in probing the crystalline structure of material. In 1912, due to having the similar order of spacing between atoms in crystal structure as an x-ray wavelength, Max von Lau and co-worker found that crystalline substance can be as used as 3D grating for X-ray. These X-rays are generated when high energetic electron beam strikes at cathode leading to the ejection of K-shell electron from its orbit. This vacant orbit is occupied by high energy electron resulting the emission of X-ray photon. Copper is the frequently used cathode for generation of x-rays of wavelength 1.54060 A°. In addition, other elements such as Fe, Cr, Mo are also used as cathode. In this way, PXRD become a very important non-destructive, and now a common analytical technique to

get information about the crystallographic structures, phases, orientations of crystal (texture), and other structural parameters like strain, crystal defects, crystallinity and crystallite size,. In this technique X-ray beam is irradiated at a sample; diffracted X-ray beam is fallen on the detector at particular angle to record the PXRD pattern. The intensity of diffracted X-rays diffraction is dependent on the constructive interference of monochromatic x-ray beam and sample and it is determined with respect to the diffraction angle  $2\theta$ .

In order to get the constructive inference resulting of interaction between incident beam and sample, Bragg's law must be satisfied (**figure 4**).

#### Bragg's law

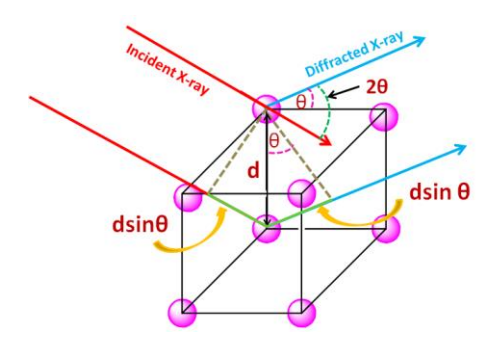


**Figure 4.** Shematic diagram of x-ray diffraction from the lattice planes.

$$2d \sin \theta = n\lambda \tag{1}$$

Where d, n,  $\theta$ ,  $\lambda$  are the spacing of lattice plane, any integer representing the order of the X-ray, scattering angle, X-ray wavelength. From the PXRD pattern, lots of information can be extracted such as purity of material, crystallite size, and arrangement of atoms, cell parameter and lattice strain. For the highly crystalline or bigger size of particle very sharp peaks appear, while in case of amorphous or smaller size of particles, peaks are becoming broader. Crystallite size of sample can be determined using the Debye-Scherrer equation.  $^{46}$ 

$$D = \frac{k\lambda}{\beta \cos\theta} \tag{2}$$

Where, k is a constant (0.9),  $\lambda$  is the incident x-ray wavelength (1.54060 A°), D is the crystallite size of particle,  $\beta$  is the full width with half maxima and  $\theta$  is diffraction angle of x-ray.

Generally the broadening of the diffraction peaks depends upon crystallite size and lattice strain. Lattice strain of the nanoparticles can be calculated using Williamson and Hall method:<sup>46</sup>

$$\frac{\beta \cos \theta}{\lambda} = \frac{1}{D} + \eta \frac{\sin \theta}{\lambda} \tag{3}$$

Where, D,  $\beta$ ,  $\lambda$ ,  $\theta$ ,  $\eta$  are the crystallite size, FWHM, wavelength of X-rays (~1.54060A° for Cu K $\alpha$  line), angle of diffraction, and lattice strain respectively. The sign of lattice strain depicts the nature of strain. If the sign of magnitude is negative (-) it shows the compressive strain, while positive sign (+) represents the tensile strain.

Bruker D8 Advance with Cu-K $\alpha$  radiation was used for PXRD measurement mentioned in this thesis.

#### 2.2.2. Scanning electron microscopy (SEM) and field emission SEM (FESEM)

Development of nanotechnology obliged the advancement of electron microscopy technique for better understanding the material properties. Scanning electron microscope (SEM) is a type of electron microscopic technique in which images of the sample is captured by scanning the sample with high energy electron beam in raster scan pattern. <sup>47,48</sup> During the

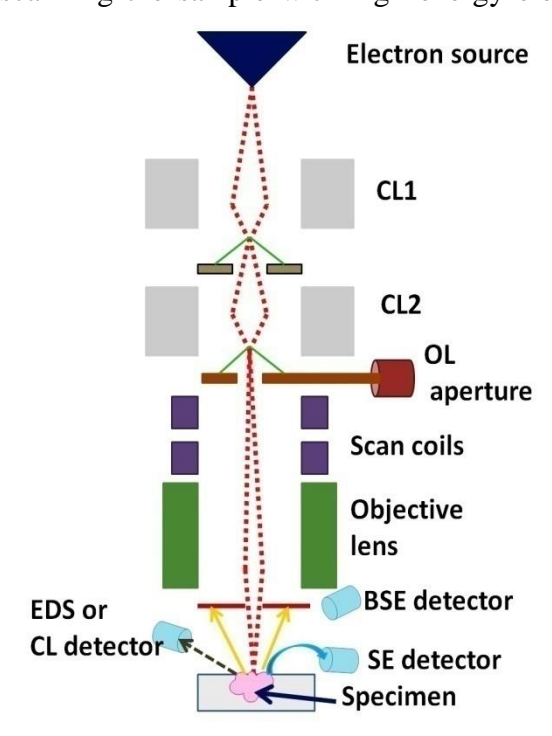


**Figure 5.** Schematic diagram of scanning electron microscope (SEM).

measurement, high energetic electron beam interacts with the atoms comprising the sample, and then generates the signals which give the information about the nature of sample such as surface topography, composition of material and electrical conductivity. Electron gun is the very important part of typical SEM because it provides the large and stable current in small beam. There are two types of emitters are used as source of electron beam: thermoionic and field emitters, which create fundamental difference between Scanning electron microscope (SEM) and Field

Emission Scanning Electron Microscope (FE-SEM). Electric current is used to heat up

the thermoionic emitter and most common materials used as thermoionic emitter are tungsten

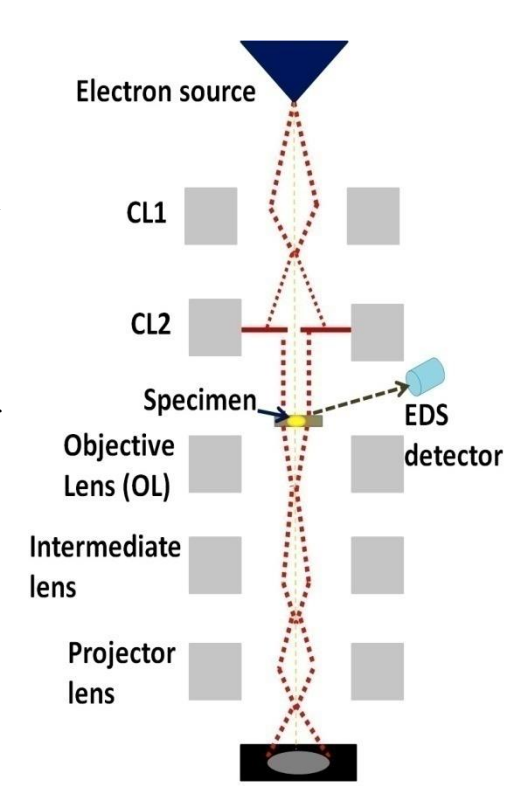
filament and lanthanum hexaboride (LaB<sub>6</sub>). The cathode is heated up enough to overcome the work function of filament leading to release of the electrons. The major limitations of thermionic sources are relatively low brightness, evaporation of cathode material and thermal drift during operation. However, such kinds of issues are not found in electron generated by Field Emission. On the other hand, in case of Field Emission Source (FES) which is also known as a cold cathode field emitter, heating of filament is not required. Here, emission of electron is taken place by producing the high electrical potential gradient around the filament. Very sharp pointed Tungsten wire with radius about (~100 nm) is used in the FES to produce extremely high potential gradient, so that work function of the electrons can be lowered down to leave the cathode. To improve the image quality significantly, FE source produces electron beam of about 1000 times smaller compared to the typical SEM. To improve resolution of sample surface, beam diameter must be smaller than the feature. On other hand, resolution can be improved ~2 nm to ~1 nm by increasing the energy from 1keV to 15keV respectively. With advancement of SEM, FE source as well as secondary electron detector is attached in the typical SEM. Huge accelerating voltage in the order of magnitude of 0.5 to 30 kV is applied between cathode and anode. In column chamber of microscope, the apparatus is kept under the extreme vacuum of about 10<sup>-6</sup> Pascal. In order to concentrate electron beam on the very small area, electromagnetic condenser lenses are attached in the column chamber (**Figure 5**). Furthermore, when the primary electron beam is allowed to interact with sample, electron energy is lost due to repeated random scanning and absorption by specimen which is also called interaction volume. Therefore, there are many factors which influence the interaction volume such as electron's landing energy, the atomic number of the specimen and the specimen's density. As a result, several types of signals are produced in SEM for instances secondary electrons; back scattered electrons (BSE), characteristics X-rays, light (cathodoluminescence), specimen current and transmitted electrons. Back-scattered electrons beam (BSE) signal is a function of atomic number of specimen and it is generated due to elastic scattering. Therefore, BSE beam along with characteristic X-rays is used to get lots of information about the sample such as atomic number (Z) and distribution of different elements in the specimen.<sup>49</sup>

NOVA NANO SEM-450 FESEM instrument is used for analyzing the morphology of nanoparticles.

#### 2.2.3. Transmission electron microscopy (TEM)

Transmission electron microscopy (TEM) is a highly advanced electron microscopy technique. It's working principle is completely different than the scanning electron microscopy technique. In TEM, electrons beam is transmitted though the highly thin samples

resulting of interaction between electrons beam and specimen. In the column chamber possesses very powerful electromagnetic lens (objective lens) to focus the electrons beam onto the specimen. When electron beam passes through the specimen, then the formation of image occurs. TEM and HRTEM images not only provide the information about the formation of nanostructure, morphology, structural unit of particles, defects but also give insight of atomic arrangement. However, information about the crystallinity of specimen can be obtained using First Fourier Transformation patterns and selected area electron diffraction pattern. In 1931, the first TEM



was made by Max Knoll and Ernst Ruska. Same group again improved the TEM by enhancing its

**Figure 6.** Schematic diagram of transmission electron microscope (TEM).

resolving power in 1933 and the first commercial TEM was available in 1939.<sup>47,48</sup> The only difference between optical microscope and TEM is electron bean is used instead of light in TEM, so that resolution can be enhanced to many folds on reducing the wavelength of electrons beam. As a result, atomistic level of analysis of specimen can be achieved.

Generally, transmission electron microscope consist of several types of powerful electromagnetic lenses in column chamber including condenser lens (CL1 and CL2), objective lens (OL), intermediate lens and projector lens are used to focus the electron beams in particular direction (**Figure 6**). In addition, column chamber is in vacuum condition so that scattering by gas molecules can be avoided and flow of electron is smooth. Sample is kept in the middle of condenser lens and objective lens whereby electron can be transmitted through sample and 2D image is produced when un-scattered electrons beam strikes to fluorescence screen situated at the bottom part of instrument. Darkness of sample image is function of the density of specimen and types of element present in the sample. Using this instrument technique, morphology, assembly of particles especially nanoscale can be easily studied.

However, high resolution TEM is used to understand the atomistic level of defects (point, line etc) and alignment of atoms and growth mechanism of particles (nanoscale).

TEM (FEI Tecnai STWIN-T30 using 300 kV electron beam source) was used to map the shape, size and lattice structure of the nanocrystals.

#### 2.2.4. Energy dispersive X-ray (EDX)

Energy dispersive X-ray spectroscopy (EDS/ EDX) is a spectroscopic technique which is used for elemental analysis or determining the chemical composition of specimen. It is attached with SEM and TEM to gather the elemental information. This equipment detects the x-rays which are produced due to interaction between high energetic electron beam and element present in the specimen. It is very sensitive and non-destructive technique to detect element which is present in less than 0.1%. When the high energetic electron beams strike to specimen, inner most shell electrons get excited and ejected from their respective shell and as a result orbit is becoming empty. Subsequently, electron of higher energy level occupies the vacant orbit leading to emission of x-ray. In this way, generated x-ray is detected by the EDS detector which is already attached with SEM or TEM. Energy of emitted x-ray is a function of elemental composition because each element has inherent different atomic structure (binding energy of core electrons). In addition, to illustrate the elemental distribution in the specimen, x-ray mapping and line profile are used.

#### 2.2.5. Thermogravimetric (TGA) and Differential Thermal analysis (DTA)

In order to study the thermal stability of sample with a function of temperature, thermogravimetric analysis is used. In this analysis, loss of weight with respect to temperature is measured. Normally, materials are very sensitive to change in temperature. By varying the temperature of the sample, its thermal stability and amount of volatile component present in the sample can be determined. To remove any kind of impurity due to atmospheric gases, inert gases (Helium or Argon) are usually used during the measurement. To determine the apparent and precise loss of mass by the sample being measured, derivative weight loss curve is plotted as a function of temperature. This technique has wide range of applications in material science especially in determining the thermal stability of materials (polymer, inorganic materials), and extent of impurity present in the sample and determination of corrosion technique under high temperature oxidizing environment.<sup>50</sup>

On the other hand, in case of Differential thermal analysis (or DTA), sample and inert reference (alumina Al<sub>2</sub>O<sub>3</sub>) are heated or cooled under the similar conditions, and then change of heat of the sample with respect to reference is plotted against time or temperature. That is called DTA curve or thermogram. Endothermic or exothermic changes are detected as compared to the inert reference. Using this technique, glass transitions, sublimation, crystallization and melting of the sample can be measured. Area under the DTA curve indicates the enthalpy change which is not influenced by the heat capacity of sample.

In present thesis, TG/DTA was measured using the Mettler Toledo Thermal Analyzer.

#### 2.2.6. BET (Brunner-Emmett- Teller) surface area analyzer

BET surface area analyzer is a very important instrumental technique for analyzing the nature of the surface of the material. The fundamental working of this instrument is a function of BET theory which was proposed by Stephen Brunauer, Paul Emmet and Edward Teller in 1938 and it measures the adsorption of gas molecules onto the surface of the materials.<sup>51</sup> There are two modes of measurement available; one is single point measurement in which at particular concentration of gases mixture (He and  $N_2$ ) is used, while in the multipoint measurement, concentration of  $N_2$  can be changed by varying the He gas concentration. By plotting the graph between volume adsorbed  $\nu s$  pressure applied at constant temperature (isothermal condition), one can get different types of isotherms with is related to the nature of material. Furthermore, it is not only used to measure the specific surface area ( $m^2/g$ ) of the materials, but it can also be used to measure pore size and pore volume of the material.

In present thesis, Bellsorp MR6, Japan instrument was used for measuring the specific

### 2.2.7. UV-Vis spectroscopy

surface area.

This spectroscopy technique is used to study the optical absorption / transmittance /reflectance of material in UV to visible region of electromagnetic wave. Generally, electronic transition of the materials is fundamentally taken place by the absorption of UV-Visible light. Absorption and emission spectra of sample is dependent on the composition, specially the semiconductor and organic based semiconductor and dye molecules which absorb the wide range of UV-Vis region of light. It is accounted to be presence of various electronic energy levels. In semiconductors, these energy levels can be designated as filled valance band (VB) and empty conduction band (CB), separation between these energy levels is known as band gap. However, in case of organic molecules, it is indicated as highest

occupied molecular orbitals (HOMO) and lowest unoccupied molecular orbitals (LUMO). On changing the size in semiconductors or conjugation bond length in organic molecules, absorption position is changed. UV-Visible spectrophotometer is divided into different parts; light source (tungsten filament/gas discharge lamp), monochromator, sample chambers and detector (photomultiplier tube/ photodiodes). The spectroscopy technique is very useful for determining the  $\lambda_{max}$  and band gap of the sample. Band gap of the semiconductor is calculated using the equation 5. Size dependent shifting of absorbance / transmittance spectra of the semiconductor nanoparticles are illustrated by Brus in 1983. The Brus's equation used to measure the size of particle is expressed as,  $^{52-53}$ 

$$\Delta E_{g} = E_{g} (np) - E_{g}(bulk) = \left\lceil \frac{\left(\hbar^{2} \pi^{2}\right)}{2\mu r^{2}} \right\rceil - \left\lceil \frac{1.8e^{2}}{\xi r} \right\rceil$$
(4)

Where,  $m_e$  and  $m_h$  are the effective mass of electron and hole respectively and  $\epsilon$  is the dielectric constant. Reduced mass  $(\mu)$  of electron-hole can be determined as,

$$\frac{1}{\mu} = \frac{1}{m_a} + \frac{1}{m_b} \tag{5}$$

The value of n represents the nature of optical transition in a semiconducting material. For instances, here  $\frac{1}{2}$ , 2,  $\frac{3}{2}$  or 3 corresponds to the allowed direct, allowed indirect, forbidden direct and forbidden indirect transitions respectively. The absorption coefficient ( $\alpha$ ) may be expressed as

$$\alpha = \frac{A}{h\nu} (h\nu - E_g)^n \tag{6}$$

Where, A is an optical constant,  $E_g$  is the band gap of the semiconductor which is dependent on the value of n.

In this thesis, Agilent Cary 100 UV-Visible DRS spectrophotometer is used for UV-Vis spectra measurement.

#### 2.2.8. Fourier Transform Infrared Spectroscopy

When the infrared region ( $100\mu m$ - $1\mu m$ ) of electromagnetic waves is used for the analysis of the sample, infrared spectroscopy is very essential tool for analyzing and studying the functional group of compounds or materials. The fundamental principle of this spectroscopy is that molecules usually consist of atoms which vibrate about their mean

position leading to the change in the resulting dipole moment of molecules. Periodic change in dipole moment enables the molecules for absorbing the infrared region of light.

Basically infrared regime of electromagnetic spectrum can be further classified into three ranges; near infrared, mid infrared and far infrared. Near IR is the high energy electromagnetic wave in which wavelength is in the range of 1.4 to 0.8  $\mu$ m (14000-4000 cm<sup>-1</sup>). However, wavelength range of mid IR and far IR are found in 4000-400 cm<sup>-1</sup> (30–1.4  $\mu$ m) and 400-10 cm<sup>-1</sup> (1000–30  $\mu$ m) respectively. The region of IR in the range 500 to 1500 cm<sup>-1</sup> is called fingerprint region and all the bending patterns are found in this region and obviously it is different for different compounds. Usually, the harmonic vibration or overtone vibration is occurred due to excitation via near IR region of electromagnetic spectrum. Vibrational frequency depends on the different factors like force constant (k) of bond and reduced mass ( $\mu$ ) of the system and relation between force constant, reduced mass and vibrational frequency can be expressed as:

$$\gamma = \frac{1}{2\pi} \sqrt{\frac{k}{\mu}} \tag{7}$$

Where k and  $\mu$  are the force constant and reduced mass respectively.

In this thesis, FTIR-8400S SHIMADZU is used for analyzing the samples.

#### 2.2.9. Photoluminescence spectroscopy

There are several types of luminescence processes have been discovered. When substance is excited using the light, radiative transition in the form of emission is occurred and it is called photoluminescence. It is fundamentally occurred due to availability of numerous excited energy levels in the material. Luminescence can be further divided into two categories-fluorescence and phosphorescence which is dependent on the types of excited states engaged in the system such as singlet and triplet. The mechanism of electronic transition can be illustrated using the Jablonski diagram which was proposed by Polish physicist Alexander Jablonski. Ground state is basically singlet (denoted by  $S_0$ ), whereas there are two excited state are situated, referred as singlet ( $S_1$ ,  $S_2$ ,  $S_3$ ...) and triplet ( $T_1$ ,  $T_2$ ,  $T_3$  and so on). Triplet excited state is relatively more stable than the singlet excited state. If the electronic transition is taken place from  $S_0$  to  $S_1$ ,  $S_2$  and so on, then there are two possibilities for returning to ground state ( $S_0$ ) from excited state. First, through internal conversion process, excited electron comes to lowest energy level of excited state and from there it come

to GS via releasing excess energy (via radiative transition), which is called fluorescence and its emission rate and life time are found in  $10^8$  s<sup>-1</sup> and pico or femto second respectively. There are several compounds or molecules such as organic dyes like eosin, fluorescin, compounds like chlorophyll, ultramarine; riboflavin, etc. show fluorescence either in visible light or in ultraviolet light.

However, in another possibility, electron might be jumped to triplet excited state via non-radiative intersystem crossing, in which spin of electron is inverted. Form this excited state, it comes to the ground state through radiative emission, and then it is called phosphorescence. Phosphorescence emission rate is occurred in  $10^3$  to  $100s^{-1}$  and its life times are typically found in milliseconds to seconds.<sup>54</sup> Rare-earth ion doped materials are the example of phosphorescence.

Edinburgh Instruments FLSP 920 spectrofluorometer attached with 450 W Xe lamp as the excitation source for steady state measurement. Life time measurements were carried out using microsecond flash lamp. HORIBA JOBIN YVON made Fluoromax-4 spectrometer, Serial No.: 1231D-0614-FM is also used in this thesis.

#### **2.2.10.** Time resolved spectroscopy

To understand the dynamic process in the materials or compounds, time resolved spectroscopic technique is very useful. In material science, this technique is substantially utilized to illustrate the mechanism of decay dynamics. Often, material is initially illuminated using the pulsed laser so that electron can be populated to different excited states. Afterwards, decay time can be measured. Generally the decay time scale can be measured from few seconds to  $10^{-15}$  seconds.

Presently, time-correlated single-photon counting technique is frequently used to perform the time-domain measurements. These instruments use high repetition rate mode-locked picosecond (ps) or femtosecond (fs) laser light source, and high-speed microchannel plate (MCP) photomultiplier tubes (PMT). For many applications, these expensive systems are being rapidly replaced by systems using pulsed laser diodes (LDs), light emitting diodes (LEDs), and small, fast PMTs.<sup>54</sup>

The following expression was used to analyze the experimental time-resolved luminescence decays:

$$P(t) = b + \sum_{i}^{n} \alpha_{i} \exp\left(\frac{-t}{\tau_{i}}\right)$$
 (8)

Where n is the number of discrete emissive species, b is a baseline correction ("DC" offset), and  $\alpha_I$  and  $\tau_i$  are the pre exponential factors and excited-state luminescence decay times associated with the i<sup>th</sup> component, respectively. For biexponential decays, the average decay time, $<\tau>$ , was calculated from

$$\langle \tau \rangle = \sum_{i=1}^{2} \alpha_i \tau_i^2 / \sum_{i=1}^{2} \alpha_i \tau_i \tag{9}$$

In this thesis, for lifetime measurements of the Eu ions, microsecond flash lamp is used. The goodness of the fit was checked by evaluating  $\chi^2$  from a plot of weighted residuals and an autocorrelation function. Later, decay times were recorded in a Edinburgh Instruments FLSP 920 spectrofluorometer spectrometer, using a solid sample holder at room temperature.

#### References

- 1 J. A. Dahl, B. L. S. Maddux and J. E. Hutchison, *Chem. Rev.* 2007, **107**, 2228-2269.
- **2** R. D. Rogers and K. R. Seddon, *Science*, 2003, **302**,792.
- 3 T. Welton, Chem. Rev., 1999, 99, 2071-2084.
- 4 N. V. Plechkova and K. R. Seddon, *Chem. Soc. Rev.*, 2008, **37**, 123–150.
- **5** B. Chen, Y.- M. Koo, D. R. MacFarlane and Z. Lei, *Chem. Rev.* 2017, **117**, 6633–6635.
- **6** K. R. Seddon, J. Chem. Tech. Biotechnol. 1997, **68**, 351-356.
- 7 M. Armand, F. Sndres, D. R. MacFarlane, H. Ohno and B. Scrosati, *Nature Mater*. 2009, **8**, 621.
- **8** M.-D. Bermúdez, A.-E. Jiménez, J. Sanes and F.-J. Carrión, *Molecules* 2009, **14**, 2888-2908.
- **9** I. Krossing, J. M. Slattery, C. Daguenet, P. J. Dyson, A. Oleinikova and H. Weingärtner, *J. Am. Chem. Soc.* 2006, **128**, 13427-13434.
- 10 D. R. MacFarlane, N. Tachikawa, M. Forsyth, J. M. Pringle, P. C. Howlett, G. D. Elliott, J. Davis, M. Watanabe, P. Simon and C. A. Angell, *Energy Environ. Sci.*, 2014, 7, 232-250.
- 11 J. S. Wilkes, J. Mol. Catal. A: Chem. 2004, 214, 11–17.
- **12** M. C. Buzzeo, R. G. Evans and R. G. Compton, *ChemPhysChem* 2004, **5**, 1106-1120.
- **13** R. K. Sharma, A.-V. Mudring and P. Ghosh, *J. Lumin.*, 2017, **189**, 43-66.

- X. Duan, J. Ma, J. Lianc and W. Zheng, *CrystEngComm*, 2014, **16**, 2550
- 15 J. S. Wilkes and M. J. Zaworotko, J. Chem. Soc., Chem. Commun., 1992, 965–967.
- S. Dai, Y. Ju, H. Gao, J. Lin, S. Pennycook and C. Barnes, *Chem. Commun.*, 2000, 243–244
- J. Dupont, G. S. Fonseca, A. P. Umpierre, P. F. P. Fichtner and S. R. Teixeira, *J. Am. Chem. Soc.*, 2002, **124**, 4228–4229.
- E. R. Cooper, C. D. Andrews, P. S. Wheatley, P. B. Webb, P. Wormald and R. E. Morris, *Nature*, 2004, **430**, 1012–1016.
- **19** A. Taubert, *Angew. Chem., Int. Ed.*, 2004, **43**, 5380–5382.
- P. S. Campbell, C. C. Santini, D. Bouchu, B. Fenet, K. Philippot, B. Chaudret, A. A. H. Pádua and Y. Chauvin, *Phys. Chem. Chem. Phys.*, 2010, **12**, 4217–4223
- 21 E. Boros, M. J. Earle, M. A. Gı^lea, A. Metlen, A-V. Mudring, F. Rieger, A. J. Robertson, K. R. Seddon, A. A. Tomaszowska, L. Trusov and J. S. Vyle, *Chem. Commun.*, 2010, 46, 716–718.
- 22 H. Itoh, K. Naka and Y. Chujo, J. Am. Chem. Soc., 2004, 126, 3026-3027.
- Y. Hatakeyama, M. Okamoto, T. Torimoto, S. Kuwabata and K. Nishikawa, *J. Phys. Chem. C*, 2009, **113**, 3917-3922.
- C. W. Scheeren, G. Machado, S. R. Teixeira, J. Morais, J. B. Domingos and J. Dupont, *J. Phys. Chem. B* 2006, **110**, 13011-13020
- K-S. Kim, D. Demberelnyamba and H. Lee, *Langmuir*, 2004, **20**, 556-560.
- 26 J. Krämer, E. Redel, R. Thomann and C. Janiak, Organometallics, 2008, 27, 1976-
- X. Zhou, T. Wu, K. Ding, B. Hu, M. Hou and B. Han, *Chem. Commun.*, 2010, **46**, 386–388.
- 28 P. S. Campbell, C. Lorbeer, J. Cybinska and A.-V. Mudring, *Adv. Funct. Mater.* 2013, 23, 2924-2931.
- Q. Ju, P. S. Campbell and A.-V. Mudring, *J. Mater. Chem. B*, 2013, **1**, 179.
- X. Liu, J. Ma, P. Peng and W. Meng, *Langmuir*, 2010, **26**, 9968–9973.
- **31** X. Duan, X. Liu, Q. Chen, H. Li, J. Li, X. Hu, Y. Li, J. Ma and W. Zheng, *Dalton Trans.*, 2011, **40**, 1924–1928.
- P. Ghosh and A.-V. Mudring, *Nanoscale*, 2016, **8**, 8160-8169
- J. Cybinska, C. Lorbeer, E. Zych and A.-V. Mudring, *ChemSusChem* 2011, **4**, 595 598.
- J. Xia, S. Yin, H. Li, H. Xu, Y. Yan and Q. Zhang, *Langmuir*, 2011, **27**, 1200–1206.

- 35 J. Xia, S. Yin, H. Li, H. Xu, L. Xu and Y. Xu, Dalton Trans., 2011, 40, 5249–5258
- R. A. Laudise, "Hydrothermal Synthesis of Crystals". C&EN September 1987, **28**, 30–43.
- A. Rabenau, The Role of Hydrothermal Synthesis in Preparative Chemistry, *Angew. Chem. Int. Ed. Engl* 1985, **24**, 1026-1040.
- X. Li, Y. Gao, L. Yu and L. Zheng, *J. Solid State Chem.* 2010, **183**, 1423–1432.
- Y. Cui, C. Wei, J. Yang, J. Zhang and W. Zheng, *CrystEngComm*, 2016, **18**, 6245-6253.
- H. Li, W. Li, L. Ma, W. Chen and J. Wang, *J. Alloys Compd.* 2009, **471**, 442–447.
- X. Ni, Z. He, X. Liu, Q. Jiao, H. Li, C. Feng and Y. Zhao, *Mater. Lett.*, 2017, **193**, 232-235.
- X. He, J. Wang, H. Jia, R. Kloepsch, H. Liu, K. Beltrop and J. Li, *J. Power Sources* 2015, **293**, 306-311.
- Y. Cui, J. Zhang, G. Li, Y. Sun, G. Zhang and W. Zheng, *Chem. Eng. J.* 2017, **325**, 424-432.
- Y. Sun, C. Li and W. Zheng, *Crys. Grow. Des.*, 2010, **10**, 262-267.
- A.A. Bunaciu1, E. G.Udriştioiu and H.Y. Aboul-Enein, Critical Reviews in Analytical Chemistry, DOI:10.1080/10408347.2014.949616.
- P. Ghosh, A. Kar and A. Patra, *J. Appl. Phys.* 2010, **108**, 113506.
- M. Knoll, Zeitschrift für technische Physik 1935, **16**, 467–475.
- H. Ma, K-J. Shieh, T. X. Qiao, Study of Transmission Electron Microscopy (TEM) and Scanning Electron Microscopy (SEM), Nature and Science, 2006, **4**, 14-22.
- D. C. Bell and N. Erdman, Low voltage electron microscopy: Principles and Applications.
- D.F. Shriver, P. W. Atkins, *Shriver & Atkins' Inorganic Chemistry*, 4th edition, Oxford University Press, Oxford 2006, *189-190*.
- N. Hwang and A. R. Barron, Version 1.1, 2011, 0500.
- 52 L. E. Brus, J. Chem. Phys. 1983, 79, 5566.
- L. E. Brus, *J. Chem. Phys.* 1984, *80*, 4403.
- J. R. Lakowicz, *Principles of Fluorescence Spectroscopy, Third Edition, Springer*, **2006**.